Institute of Space and Aeronautical Science, University of Tokyo
Report No. 448, March 1970

Energy Transfer Processes in an Ionized Nonequilibrium Flow

By

Hiroki HONMA*

Summary: The energy transfer processes of an electron gas are investigated, both analytically and experimentally, for a pipe flow of weakly ionized nonequilibrium plasmas. An energy equation for electrons is solved for an axially symmetric flow through a circular tube for the case when the plasma density distribution in the flow is mainly controlled by ambipolar diffusion. It follows from the analysis that the electron temperature exponentially decreases along the tube axis. The decay rates of the electron temperature along the tube axis are obtained in analytical formulae for both slug and Poiseuille flows. The measurement for the decay rates is worked out for ionized argon flows in the low-density glow-discharge tube for a range of the Knudsen number for electrons around 0.1. The measured decay rates are found to be in qualitative agreement with the rates evaluated from the present analysis.

SYMBOLS

$b_j, \bar{b}_j$	eigenvalues for the diffusion equations for slug and Poiseuille flows ($j=1, 2, \cdots$)
$C_j, \bar{C}_j$	eigenvalues for the electron energy equations for slug and Poiseuille flows ($j=1, 2, \cdots$)
D_a	ambipolar diffusion coefficient
D_i	ion diffusion coefficient
e	electronic charge
$J_0(b\eta)$	Bessel function of the first kind, of order zero
k	Boltzmann constant
K_e	electron thermal conductivity
K_m	modified Kundsen number, defined by Eq. (3.1.22)
K_n	ordinary Knudsen number for electron-atom collisions
L_D	electron Lewis number, defined by Eq. (3.1.21)
m_s	particle mass of species s
n_s	number density of species s
n_p	plasma number density
P_D	ambipolar Peclet number, defined by Eq. (3.1.20)
Q_{st}	effective hard sphere cross section for particles s and t

* Chiba University, Chiba. Visiting Research Fellow at the Institute of Space and Aeronautical Science, University of Tokyo, on leave from Chiba University.

r	radial coordinate of a circular tube
R	tube radius
$S_j, \bar{S}_j$	eigenfunctions for the electron energy equations for slug and Poiseuille flows ($j=1, 2, \cdots$)
T_s	temperature of species s
u_a, v_a	axial and radial velocities of atoms
$\bar{u}_a, \bar{v}_a$	normalized axial and radial velocities of atoms
U_0	reference velocity or mean velocity of the flow through a circular tube
Y_j	eigenfunction for the diffusion equation for Poiseuille flow ($j=1, 2, \cdots$)
$Z(\eta)$	function defined by Eq. (3.2.9)
α	normalized plasma density
η	normalized radial coordinate of a circular tube
$\lambda_1, \bar{\lambda}_1$	decay rates of the plasma density along the tube axis for slug and Poiseuille flows
λ_j	index defined by Eq. (3.2.4)
$\mu_1, \bar{\mu}_1$	decay rates of the electron temperature along the tube axis for slug and Poiseuilli flows
μ_j	index defined by Eq. (3.2.11)
ξ	normalized axial coordinate of a circular tube
τ_s	normalized temperature of species s
$\bar{\phi}_f$	normalized floating potential

SUBSCRIPTS

a	atoms
e	electrons
i	ions
s	refers to species
0	refers to the quantities at a reference point or in a reference section

SUPERSCRIPT

*	refers to the quantities on the tube axis

I. INTRODUCTION

Recently, studies of ionized nonequilibrium flows have been carried out by many investigators in connection with gas dynamic problems encountered in reentry of space vehicles and MHD power generation. Here, the term *nonequilibrium* implies such a phenomenon that the electron temperature deviates from both ion and atom temperatures. Such nonequilibrium phenomena are accompanied by the rapid change of thermodynamic and/or electric properties of gases; shock transition [*1*]~[*5*], highly expanding nozzle flow [*6*]~[*9*], boundary layer [*10*]~[*16*], and so on. Moreover, such phenomena occur more and more conspicuously as gas density

decreases, since the energy exchange between electrons and heavy particles becomes less efficient. Therefore, in order to clarify the characteristics of such nonequilibrium phenomena in ionized flows, it is useful to study the energy transfer processes of an electron gas at low density; electron thermal conduction, diffusion, and so on. In the present paper, the energy transfer processes of an electron gas are investigated, both analytically and experimentally, for a pipe flow of weakly ionized nonequilibrium plasmas at low density. The electron temperature distribution in a circular tube is analytically obtained by solving the energy equation for electrons, and compared with the measured distribution. In particular, in order to estimate the effects of gas rarefaction on the energy transfer processes of an electron gas in ionized nonequilibrium flows, the electron temperature distribution along the tube axis is measured for a range of the ratio of the electron mean free path to the tube diameter (the Knudsen number for electrons) around 0.1, and compared with the distribution evaluated from the present analysis.

In the analysis, an electron gas is regarded as a continuum fluid. We consider the case when charge separation is negligible everywhere except the thin sheath close to the wall. Therefore, the plasma density distribution may reasonably be assumed to be mainly controlled by ambipolar diffusion. With the assumption of ambipolar diffusion, the continuum equations for electrons are simplified, and reduced to two equations; the diffusion equation and the energy equation.

The diffusion equation has been solved for a stationary plasma in a circular tube by Schottky [*17*] and for a plasma flow through a circular tube by Schottky and Issendorff [*18*] and Konenko [*19*]. Schottky and Issendorff [*18*] have analyzed a slug flow under the assumption of constant electron temperature. Konenko [*19*] has analyzed a diffusion flow of stationary plasma with electron temperature gradient. In the present paper, the solution obtained by Schottky and Issendorff [*18*] is applied to the analysis of slug flow and its extended solution for Poiseuille flow is presented. For weakly ionized gases, quasi-one-dimensional analyses of energy transfer processes of an electron gas in stationary plasmas in a circular tube have been made by several investigators [*20*]~[*25*]. The energy equation for electrons has been solved for unsteady one-dimensional heat conduction along the tube axis [*20*]~[*23*] or radial energy transport in the tube section [*24*],[*25*]. It is not always expected that quasi-one-dimensional analysis can be applied to the present problem, because in general the plasma density and the electron temperature vary in both axial and radial directions. Therefore, in the present paper, the energy equation for electrons is solved for axially symmetric flow for both cases of slug and Poiseuille flows.

The measurements of the electron temperature distribution along the tube axis have been made by Randall and Webb [*26*] for a mercury afterglow in the flow through a circular tube, by Baranov and Vasil'eva [*27*] for an arc in a pipe flow of argon and by Konenko [*28*] for a diffusion flow of stationary helium plasma, respectively. In the experiment of mercury afterglow [*26*], the plasma density distribution in the flow is estimated to be mainly controlled by recombination processes. In the experiment of argon arc [*27*], the electron temperature has been measured for

an arc deformed by the flow. In the present analysis, only diffusion process is taken into account, and the net current is assumed to be zero. Therefore, the results of both first and second experiments cannot be compared with the results of the present analysis. Only the electron temperature distribution measured by Konenko [*28*] can be compared with the distribution evaluated from the present analysis. As will be seen later, the experimental conditions of Konenko [*28*] correspond to the case when the Knudsen number for electrons is very small. In the present paper, the electron temperature distribution is measured in a pipe flow of weakly ionized nonequilibrium argon, and compared with the distribution evaluated from the present analysis. The test gas (argon) around 1 Torr in pressure is weakly ionized by a glow discharge and ejected through a circular tube. Experimental conditions correspond to the Knudsen number for electrons around 0.1.

II. Historical Survey

In this chapter, the works associated with the analysis of the pipe flow of weakly ionized nonequilibrium plasmas are surveyed. First a survey is made for continuum approach of the positive column of a gas discharge, since the analysis for plasma density distribution in the flow is closely related to that of the positive column. Several authors have analytically obtained the density distribution of charged particles in quiescent, weakly ionized gases confined by cold walls in order to clarify the structure of the positive column of a gas discharge. In 1924, Schottky [*17*] analyzed this problem under the assumption that quasi-neutrality holds everywhere in the tube. In 1954, Allis and Rose [*29*] took into account the sheath in the neighborhood of the wall, and in 1965 Cohen and Kruskal [*30*] have extensively developed the work of Allis and Rose [*29*] in a more rigorous mathematical treatment. In Schottky's analysis [*17*] the ion drift velocity becomes infinite at the wall. In 1949, Bohm [*31*] suggested a criterion that the ion drift velocity should be less than or equal to the sound speed of the electron-ion gas (or ambipolar sound speed) in front of the boundary or the wall sheath. Furthermore, in 1962, Person [*32*] studied in detail the influence of the ion inertia on the ion drift velocity, and found that Bohm's criterion can be derived from his inertia-controlled-diffusion theory. Recently, Friedman [*33*] and Friedman and Levi [*34*] (1967) introduced the effects of both ion inertia and wall sheath into the analysis through two-fluid treatment.

In 1925, Schottky and Issendorff [*18*] analyzed a weakly ionized flow of mercury vapour through a circular tube. The equation of ambipolar diffusion was solved for the case when the radial distribution of velocity of neutral particles may be assumed to be rectangular (slug flow). Under the assumption of constant electron temperature, the plasma density distribution in the flow was obtained in an analytical formula. For the case when the electron temperature gradient must be taken into account, the diffusion equation has been solved by Konenko [*19*] (1963) for a diffusion flow of stationary plasma. A semi-empirical formula has been used for the axial distribution of the electron temperature. In taking into account both ion inertia and wall sheath, the diffusion equation has been solved by Shioda [*35*]

(1969) for flows of a weakly ionized gas between parallel cold walls on the basis of the two-fluid treatment presented by Friedman [*33*].

The survey of the works associated with the energy transfer processes of an electron gas will also be made first from that with respect to stationary plasma in discharge tubes. In 1958, Goldstein and Sekiguchi [*20*] determined the electron thermal conductivity in a decaying plasma by technique of interaction of pulsed microwaves. The plasma electrons were heated by the pulsed radio-frequency input power, and heat propagation phenomena along a discharge tube were observed. The energy equation for unsteady one-dimensional heat conduction was solved. The extended studies have been carried out by Sekiguchi and Herndon [*21*] (1958), by Rostas et al. [*22*] (1963) and by Nygaard [*23*] (1967). The first authors [*21*] have determined the electron thermal conductivity in a gaseous plasma for cases when electron-electron interaction is predominant. The second authors [*22*] have studied electron thermal conduction in a plasma with magnetic field. The last author [*23*] has determined the electron thermal diffusivity for cases when electron-atom collisions are predominant. In their studies, the equations for unsteady quasi-one-dimensional heat conduction have also been solved. In order to obtain the radial distribution of the electron temperature in a discharge tube, Pytte and Winsor [*24*] (1965) have solved the energy equation for electrons for a stationary helium plasma at pressure of one atmosphere in a cylindrical duct. It has been pointed out that the electron temperature deviates from the atom temperature in the neighborhood of the duct wall. Furthermore, Keefer [*25*] (1967) has analytically obtained the radial distribution of the electron temperature in a circular tube for an electrodeless discharge at low pressure under the assumption that the radial energy flux of electrons is constant. In the analysis made by Pytte and Winsor [*24*], thermal conduction and diffusion have not been taken into account, since the gas pressure is high. On the contrary, in the analysis made by Keefer [*25*], the effects of ambipolar diffusion and electron thermal conduction on the energy transport have been taken into account. As for the diffusion loss of electron energy in a plasma of a gas discharge, Biondi [*36*] (1954) studied the diffusion cooling of electrons in the occurrence of afterglow of a pulsed microwave discharge. From the fact that the ambipolar diffusion coefficient decreases as the gas pressure decreases, it has been demonstrated that under certain circumstances the average kinetic energy of electrons in an ionized gas may decrease below that of atoms.

In 1935, Randall and Webb [*26*] studied factors determining the time rate of decrease of the electron temperature in the mercury afterglow in the flow through a circular tube. Langmuir's probe theory (free-molecule thory) was applied to the analysis of the energy transfer processes of an electron gas in the flow. It was suggested that the rate of decrease of the electron temperature would mainly depend on the thermal conduction process. The energy equation for an axially symmetric flow has been used by Baranov and Vasil'eva [*27*] (1965) only for crude evaluation of energy transfer processes of an electron gas for an arc in a pipe flow of argon.

The various boundary conditions for the electron temperature at the wall have been applied to the analyses of ionized nonequilibrium boundary layers. In the

case of highly ionized gases, Jukes [*10*] (1956) took into account the sheath close to the wall and specified condition at the sheath edge. The electron gas was assumed to be a continuum fluid outside of the sheath and collisionless in the sheath. The outer and inner solutions are matched such that the energy flux of electrons is continuous at the sheath edge. This matching condition has been used by many investigators [*11*]~[*14*]. In the case of weakly ionized gases, another condition has been presented by Chung [*16*] (1965). In his analysis, the electron gas is assumed to be a continuum fluid in the sheath, and so the boundary condition is specified at the wall. In the case of weakly ionized gases, the electron thermal conductivity is proportional to the electron density. Therefore, if the electron density is assumed to vanish at the wall surface, the coefficient of the second derivative of the electron temperature with respect to the space coordinate vanishes there. Chung [*16*] imposed the condition that the second derivative is finite at the wall surface. Recently, properties of electrons near absorbing and emitting surface have been studied by Chung [*37*] (1969) for weakly ionized plasmas by analyzing the Boltzmann equation governing the electrons. From the analysis it was found that the simple surface boundary condition for the electron energy equation employed by Chung [*16*] in the continuum plasma analysis is correct in the limit of no surface emission, which corresponds to the case of vanishing value of the electron density at the wall surface. If the wall ion sheath is taken into account, the analysis of two- or three-dimensional boundary layer becomes very complicated. Therefore, only one-dimensional cases have been analyzed for ionized nonequilibrium boundary layers. Recently, a two-dimensional boundary layer has been analyzed by Sherman and Reshotko [*14*] (1969) by applying the local similarity analysis.

III. An Analysis of a Pipe Flow of Weakly Ionized Nonequilibrium Plasmas

3.1 Mathematical Formulation

3.1.1 *Basic Assumptions*

The analysis is based on the following assumptions.

a) Singly ionized: The gas is assumed to be a ternary mixture of atoms, singly charged ions and electrons.

b) Weakly ionized: The number fractions of ions and electrons are assumed to be so small that the thermodynamic properties and the flow velocity of a gas as a whole are not affected to any appreciable degree by the presence of ions and electrons. The collisions between the charged particles are neglected.

c) Quasi-charge-neutrality: Charge separation is assumed to be negligible everywhere except thin sheath close to the wall.

d) Frozen flow: The charged particles produced or lost per unit time by ionization-recombination reactions in the gas phase are assumed to be much smaller than those lost by diffusing toward the wall. The ionization-recombination reactions are ignored in the gas phase.

e) Fully catalytic wall: It is assumed that the charged particles diffusing toward the wall all recombine at the wall.

f) Without external field: External electric and magnetic fields are not applied. The net current is assumed to be zero.

g) Elastic collisions: It is assumed that the charge particles mainly elastically collide with atoms.

h) High electron temperature: The electron temperature is assumed to be much higher than the atom and ion temperatures. However, the value of the electron temperature should be restricted within a moderate range by the assumptions of frozen ionization and elastic collisions, because these assumptions become invalid for the excessively high electron temperature. The ion and atom temperatures are assumed to be nearly equal to the room temperature.

3.1.2 *Basic Equations*

On the basis of the analysis made by Burgers [*38*] and Jaffrin [*3*], the following equations for ions and electrons are obtained. The conservation of mass for ions and electrons yields

$$\operatorname{div}(n_s \boldsymbol{V}_s)=0, \quad (s=i, e). \tag{3.1.1}$$

The energy equation for electrons is

$$n_e \boldsymbol{V}_e \cdot \operatorname{grad}\left(\frac{5}{2}kT_e\right)-\operatorname{div}(K_e \operatorname{grad} T_e)$$
$$-en_e \boldsymbol{V}_e \cdot \operatorname{grad}\phi+\nu_{ea}(T_e-T_a)=0. \tag{3.1.2}$$

The kinetic energy and viscous dissipation of the electron gas are neglected in Eq. (3.1.2), since their contribution to the energy transfer processes can be neglected due to small mass of an electron. On the basis of the assumptions c) to f) of the preceding section, the drift velocities $\boldsymbol{V}_i$ and $\boldsymbol{V}_e$ of ions and electrons are assumed to be expressed by

$$n_i(\boldsymbol{V}_i-\boldsymbol{V}_a)=n_e(\boldsymbol{V}_e-\boldsymbol{V}_a)=-D_a \operatorname{grad} n_p, \tag{3.1.3}$$

where n_p denotes the plasma density in a quasi-neutral plasma. Equation (3.1.3) denotes the ambipolar diffusion flux. If the electron temperature gradient is taken into account for the diffusion flux, the term $-D_i n_p \operatorname{grad}(T_e/T_a)$ should be added to the right hand side of Eq. (3.1.3) [*12*],[*16*]. In the present analysis, we consider only the plasma density gradient for the diffusion flux in order to evaluate the effects of ambipolar diffusion on the electron energy transport from the simplified analysis. Furthermore, on the basis of the assumption of the preceding section, we obtain the expression for the space potential ϕ from the generalized Ohm's law

$$\operatorname{grad}\phi=\frac{k}{en_p}\operatorname{grad}(n_p T_e). \tag{3.1.4}$$

Substituting Eqs. (3.1.3) and (3.1.4) into Eqs. (3.1.1) and (3.1.2), we obtain

$$V_a \cdot \text{grad}\, n_p = \text{div}(D_a \,\text{grad}\, n_p), \tag{3.1.5}$$

$$\begin{aligned}(n_p V_a - D_a \,\text{grad}\, n_p)\cdot \text{grad}\left(\frac{3}{2}kT_e\right) - \text{div}(K_e \,\text{grad}\, T_e)\\ - kT_e n_p[V_a \cdot \text{grad}(\ln n_p) - D_a\{\text{grad}(\ln n_p)\}^2]\\ + \nu_{ea}(T_e - T_a) = 0.\end{aligned} \tag{3.1.6}$$

With the dissipation and transfer coefficients D_a, K_e and ν_{ea} assumed to be known functions of the dependent variables, then Eqs. (3.1.5) and (3.1.6) constitute a system of equations for two unknowns n_p anb T_e. For cylindrical coordinates illustrated in Fig. 3-1, Eqs. (3.1.5) and (3.1.6) become

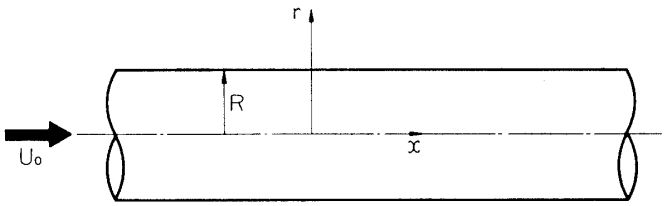

FIG. 3-1. Flow through a circular tube.

$$u_a \frac{\partial n_p}{\partial x} + v_a \frac{\partial n_p}{\partial r} = \frac{\partial}{\partial x}\left(D_a \frac{\partial n_p}{\partial x}\right) + \frac{D_a}{r}\frac{\partial n_p}{\partial r} + \frac{\partial}{\partial r}\left(D_a \frac{\partial n_p}{\partial r}\right), \tag{3.1.7}$$

$$\begin{aligned}&\frac{3}{2}k\left\{n_p u_a \frac{\partial T_e}{\partial x} + n_p v_a \frac{\partial T_e}{\partial r} - D_a\left(\frac{\partial n_p}{\partial x}\frac{\partial T_e}{\partial x} + \frac{\partial n_p}{\partial r}\frac{\partial T_e}{\partial r}\right)\right\}\\ &- \frac{\partial}{\partial x}\left(K_e \frac{\partial T_e}{\partial x}\right) - \frac{1}{r}\frac{\partial}{\partial r}\left(rK_e \frac{\partial T_e}{\partial r}\right)\\ &- kT_e n_p\left[u_a \frac{\partial \ln n_p}{\partial x} + v_a \frac{\partial \ln n_p}{\partial r} - D_a\left\{\left(\frac{\partial \ln n_p}{\partial x}\right)^2 + \left(\frac{\partial \ln n_p}{\partial r}\right)^2\right\}\right]\\ &+ \nu_{ea}(T_e - T_a) = 0.\end{aligned} \tag{3.1.8}$$

3.1.3 *Dissipation and Transfer Coefficients*

As for the energy transfer coefficient ν_{ea} and the electron thermal conductivity K_e, the formulae evaluated by Jaffrin [3] are used. The transfer coefficient ν_{ea} is expressed as

$$\nu_{ea} = 8\sqrt{2}\, k n_e \frac{n_a Q_{ea}(T_e)}{m_a}\sqrt{\frac{m_e kT_e}{\pi}}, \tag{3.1.9}$$

where $Q_{ea}(T_e)$ is the effective hard sphere cross section for electron-atom collisions, defined by

$$Q_{ea}(T_e) = \frac{1}{2}\int_0^\infty \sigma(\varepsilon)\left(\frac{\varepsilon}{kT_e}\right)^2 \exp\left(-\frac{\varepsilon}{kT_e}\right) d\left(\frac{\varepsilon}{kT_e}\right). \tag{3.1.10}$$

The quantity $\sigma(\varepsilon)$ is the momentum-transfer cross section for a monoenergetic beam of electrons in which ε is the energy of a single electron, and can be obtained

from theoretical and experimental data [*39*]. Equations (3.1.9) and (3.1.10) are obtained from the collision integral of the Boltzmann equation by assuming that the velocity distribution functions for electrons and atoms are Maxwellian, and that the energy transfer due to electron-atom collisions is equated to the effective energy transfer for hard sphere interactions. The same expression as Eq. (3.1.9) has also been obtained by Morse [*40*]. Equation (3.1.10) has also used by Daiber and Waldron [*41*] to obtain scattering cross sections of argon and atomic oxygen to thermal electrons.

The electron thermal conductivity is expressed from the Fay's mixture law [*42*] for weakly ionized gases as

$$K_e=\frac{75}{64}\frac{kn_e\sqrt{\pi kT_e/m_e}}{\sqrt{2}\,n_aQ_{ea}}. \tag{3.1.11}$$

It has experimentally been shown by Nygaard [*23*] that the electron thermal conductivity is proportional to the electron density for weakly ionized gases. In his experiment, the electron thermal diffusivity has been determined in a room temperature neon afterglow plasma. It has been found that the electron thermal diffusivity is independent of the electron number density and that it agrees within 25% with Shkarofsky's theory [*43*].

In general, the ambipolar diffusion coefficient D_a is expressed as

$$D_a=D_i(T_e/T_a+1). \tag{3.1.12}$$

For argon, we use the semi-empirical formula given by [*27*]

$$D_a=0.138\,T_e/p_a,$$

where T_e denotes the electron temperature in °K, p_a the atom pressure in Torr and D_a the ambipolar diffusion coefficient in cm²/sec.

3.1.4 *Boundary Conditions*

It is assumed that the radial profiles of the plasma density and the electron temperature are given at the section $x=0$;

$$n_p(0,r)=n_0(r),\quad T_e(0,r)=T_0(r), \tag{3.1.13}$$

where the origin of x is fixed at an arbitrary section of the circular tube. For $x\to\infty$, the values of the plasma density and the electron temperature should be finite;

$$n_p, T_e;\ \text{finite},\quad \text{at } x\to\infty. \tag{3.1.14}$$

On the axis of the tube, the axially symmetric conditions are given by

$$\frac{\partial n_p}{\partial r}=0,\quad \frac{\partial T_e}{\partial r}=0,\quad \text{at } r=0. \tag{3.1.15}$$

On the basis of the assumption of fully catalytic wall, the plasma density is assumed to be zero at the wall;

$$n_p=0, \quad \text{at } r=R. \tag{3.1.16}$$

The coefficient of the highest order term of Eq. (3.1.8) vanishes as $r\to R$, because the electron thermal conductivity approaches zero with n_p. Moreover, the term $\partial \ln n_p/\partial r$ of Eq. (3.1.8) diverges as $r\to R$. Therefore, Eq. (3.1.8) has a singularity at $r=R$. However, the value of the electron temperature should be finite;

$$T_e; \text{ finite}, \quad \text{at } r=R. \tag{3.1.17}$$

The characteristics of the singularity of Eq. (3.1.8) at $r=R$ will be discussed later.

3.1.5 *Normalized Equations*

The variables n_p, T_e, x and r are normalized by

$$\alpha=n_p/n_{p0}, \quad \tau_e=T_e/T_{e0}, \quad \xi=x/R, \quad \eta=r/R,$$

where the subscript 0 denotes the values at the reference point. The normalized equations for Eqs. (3.1.7) and (3.1.8) are

$$\bar{u}_a\frac{\partial\alpha}{\partial\xi}+\bar{v}_a\frac{\partial\alpha}{\partial\eta}=\frac{\partial}{\partial\xi}\left(\frac{1}{P_D}\frac{\partial\alpha}{\partial\xi}\right)+\frac{1}{\eta}\frac{\partial}{\partial\eta}\left(\frac{\eta}{P_D}\frac{\partial\alpha}{\partial\eta}\right), \tag{3.1.18}$$

$$\begin{aligned}&\frac{3}{2}\left\{\alpha\left(\bar{u}_a\frac{\partial\tau_e}{\partial\xi}+\bar{v}_a\frac{\partial\tau_e}{\partial\eta}\right)-\frac{1}{P_D}\left(\frac{\partial\alpha}{\partial\xi}\frac{\partial\tau_e}{\partial\xi}+\frac{\partial\alpha}{\partial\eta}\frac{\partial\tau_e}{\partial\eta}\right)\right\}\\&-\left\{\frac{\partial}{\partial\xi}\left(\frac{\alpha}{P_DL_D}\frac{\partial\tau_e}{\partial\xi}\right)+\frac{1}{\eta}\frac{\partial}{\partial\eta}\left(\frac{\alpha\eta}{P_DL_D}\frac{\partial\tau_e}{\partial\eta}\right)\right\}\\&-\alpha\tau_e\left[\bar{u}_a\frac{\partial\ln\alpha}{\alpha\xi}+\bar{v}_a\frac{\partial\ln\alpha}{\partial\eta}-\frac{1}{P_D}\left\{\left(\frac{\partial\ln\alpha}{\partial\xi}\right)^2+\left(\frac{\partial\ln\alpha}{\partial\eta}\right)^2\right\}\right]\\&+\frac{1}{3\pi}\left(\frac{32}{5}\right)^2\frac{\alpha}{K_m^2L_DP_D}(\tau_e-\tau_a)=0,\end{aligned} \tag{3.1.19}$$

where the atom velocities u_a and v_a and the atom temperature T_a are normalized by the reference velocity U_0 and the electron temperature T_{e0} at a reference point, respectively, as

$$\bar{u}_a=u_a/U_0, \quad \bar{v}_a=v_a/U_0, \quad \tau_a=T_a/T_{e0}.$$

The dimensionless numbers P_D, L_D and K_m are defined by

$$P_D=U_0R/D_a, \tag{3.1.20}$$

$$L_D=kn_eD_a/K_e, \tag{3.1.21}$$

$$K_m=\sqrt{m_a/m_e}\,/(n_aQ_{ea}R). \tag{3.1.22}$$

The dimensionless number P_D is the product of the Reynolds number of neutral gas flow and the Schmidt number for ambipolar diffusion $S_{ca}=\nu_a/D_a$, where ν_a is the kinematic viscosity of atoms. It is termed the Peclet number for ambipolar

diffusion or the ambipolar Peclet number. The dimensionless number L_D is 0.4 times as large as the Lewis number for an electron gas L_e; $L_e=D_a\rho_e C_{pe}/K_e$ $(=2.5L_D)$, where ρ_e and C_{pe} are the density and the specific heat of the electron gas, respectively. The number L_D is termed the electron Lewis number. Since $(n_aQ_{ea})^{-1}$ is the mean free path of electrons for electron-atom collisions, $(2n_aQ_{ea}R)^{-1}$ is the Knudsen number for electrons. The number K_m is proportional to the Knudsen number for electrons and the root of the mass ratio of an atom and an electron. It is termed the modified Knudsen number. As seen from Eqs. (3.1.18) and (3.1.19), the normalized plasma density α depends on $\bar{u}_a$, $\bar{v}_a$ and P_D, while the normalized electron temperature τ_e depends on $\bar{u}_a$, $\bar{v}_a$, P_D, L_D, K_m and τ_a.

The normalized boundary conditions are written as

$$\alpha=\alpha_0(\eta),\quad \tau_e=\tau_0(\eta), \qquad \text{at } \xi=0, \tag{3.1.23}$$

$$\alpha,\ \tau_e;\ \text{finite}, \qquad \text{at } \xi\to\infty, \tag{3.1.24}$$

$$\partial\alpha/\partial\eta=0,\quad \partial\tau_e/\partial\eta=0, \qquad \text{at } \eta=0, \tag{3.1.25}$$

$$\alpha=0,\quad \tau_e;\ \text{finite}, \qquad \text{at } \eta=1, \tag{3.1.26}$$

where $\alpha_0(\eta)$ and $\tau_0(\eta)$ are arbitrary functions to be given at $\xi=0$.

3.2 *Linearized Equations and Their Solutions*

3.2.1 *Linearized Equations*

As seen from Eqs. (3.1.9), (3.1.11), (3.1.12) and Eqs. (3.1.20) through (3.1.22), the dimensionless numbers P_D, L_D and K_m depend on the electron temperature. Therefore, in general, Eqs. (3.1.18) and (3.1.19) constitute a system of simultaneous, nonlinear equations for the dependent variables α and τ_e. Equations (3.1.18) and (3.1.19) should be solved for each gas species and for the prescribed range of the electron temperature. However, if we assume that these numbers are constant, both equations (3.1.18) and (3.1.19) are reduced to linear equations for α and τ_e as

$$P_D\left(\bar{u}_a\frac{\partial\alpha}{\partial\xi}+\bar{v}_a\frac{\partial\alpha}{\partial\eta}\right)=\frac{\partial^2\alpha}{\partial\xi^2}+\frac{1}{\eta}\frac{\partial\alpha}{\partial\eta}+\frac{\partial^2\alpha}{\partial\eta^2}, \tag{3.2.1}$$

$$\begin{aligned}&\frac{\partial^2\tau_e}{\partial\xi^2}+\left[\frac{\partial\ln\alpha}{\partial\xi}-\frac{3}{2}L_D\left(P_D\bar{u}_a-\frac{\partial\ln\alpha}{\partial\xi}\right)\right]\frac{\partial\tau_e}{\partial\xi}\\&\quad+\left\{\frac{1}{\eta}+\left(1+\frac{3}{2}L_D\right)\frac{\partial\ln\alpha}{\partial\eta}-\frac{3}{2}L_DP_D\bar{v}_a\right\}\frac{\partial\tau_e}{\partial\eta}+\frac{\partial^2\tau_e}{\partial\eta^2}\\&\quad+\left\{\left(P_D\bar{u}_a-\frac{\partial\ln\alpha}{\partial\xi}\right)L_D\frac{\partial\ln\alpha}{\partial\xi}+\left(P_D\bar{v}_a-\frac{\partial\ln\alpha}{\partial\eta}\right)L_D\frac{\partial\ln\alpha}{\partial\eta}\right\}\tau_e\\&\quad-\frac{1}{3\pi}\left(\frac{32}{5}\right)^2\frac{1}{K_m^2}(\tau_e-\tau_a)=0.\end{aligned} \tag{3.2.2}$$

Equations (3.2.1) and (3.2.2) can be solved without restriction of gas species and ranges of the electron temperature. Through simpler analyses, it becomes possible to obtain the essential features of the flow interested here.

3.2.2 *Plasma Density and Electron Temperature Distributions in Slug Flow*

First we consider a slug flow, whose radial velocity distribution of neutral particles is rectangular. If the uniform velocity of atoms is chosen as a reference velocity U_0, the normalized atom velocities are

$$\bar{u}_a = 1, \qquad \bar{v}_a = 0.$$

By means of the method of separation of variables, we obtain the elementary solutions of Eq. (3.2.1) as

$$\alpha(\xi, \eta) = \begin{Bmatrix} \exp(-\lambda\xi) \\ \exp(-\lambda'\xi) \end{Bmatrix} \begin{Bmatrix} J_0(b\eta) \\ Y_0(b'\eta) \end{Bmatrix},$$

where the functions $J_0(b\eta)$ and $Y_0(b'\eta)$ are the Bessel functions of the first and second kinds, of order zero. With the boundary conditions (3.1.23) through (3.1.26), we obtain

$$\alpha = \sum_1^\infty A_j \exp(-\lambda_j\xi) J_0(b_j\eta), \tag{3.2.3}$$

where the values of λ_j and A_j are obtained from

$$\lambda_j = 0.5 P_D(-1 + \sqrt{1 + 4b_j^2/P_D^2}), \tag{3.2.4}$$

$$A_j = \frac{2}{J_1^2(b_j)} \int_0^1 \eta \alpha_0(\eta) J_0(b_j\eta) d\eta.$$

The eigenvalue b_j is one of the roots of the equation

$$J_0(b_j) = 0, \tag{3.2.5}$$

where we define $b_1 < b_2 < \cdots$, so that we obtain $\lambda_1 < \lambda_2 < \cdots$ from Eq. (3.2.4). As ξ increases, the value of the first term of the right hand side of Eq. (3.2.3) becomes predominant except when the value of P_D is very large (because $\lambda_j \to 0$ for $P_D \to \infty$). For large ξ, we can approximately rewrite Eq. (3.2.3) as

$$\alpha = A_1 \exp(-\lambda_1\xi) J_0(b_1\eta).$$

Even if the radial profile of the plasma density is given in an arbitrary form at $\xi = 0$, it is transformed into a Bessel function $J_0(b_1\eta)$ far downstream of the origin. When we choose the initial profile of the plasma density as

$$\alpha_0(\eta) = J_0(b_1\eta), \tag{3.2.6}$$

we obtain

$$\alpha(\xi, \eta) = \exp(-\lambda_1\xi) J_0(b_1\eta). \tag{3.2.7}$$

Equation (3.2.7) is the formula derived by Schottky and Issendorff [*18*]. It will be shown in Chap. V that the radial profile of the plasma density expressed as

Eq. (3.2.6) can easily be realized in a pipe flow of weakly ionized nonequilibrium plasmas. In the expression of Eq. (3.2.7), λ_1 denotes the decay rate of the plasma density along the tube axis.

Substituting Eq. (3.2.7) into Eq. (3.2.2) and excluding the inhomogeneous term, we obtain the homogeneous equation

$$\frac{\partial^2\tau_e}{\partial\xi^2}-\left\{\lambda_1+\frac{3}{2}L_D(P_D+\lambda_1)\right\}\frac{\partial\tau_e}{\partial\xi}+\left\{\frac{1}{\eta}+Z(\eta)\left(1+\frac{3}{2}L_D\right)\right\}\frac{\partial\tau_e}{\partial\eta}$$
$$+\frac{\partial^2\tau_e}{\partial\eta^2}-\left\{\lambda_1L_D(P_D+\lambda_1)+L_DZ^2(\eta)+\frac{1}{3\pi}\left(\frac{32}{5}\right)^2\frac{1}{K_m^2}\right\}\tau_e=0, \tag{3.2.8}$$

where the function $Z(\eta)$ is defined by

$$Z(\eta)=\frac{1}{J_0(b_1\eta)}\frac{dJ_0(b_1\eta)}{d\eta}. \tag{3.2.9}$$

By means of the method of separation of variables, we obtain the solution of Eq. (3.2.8) with the boundary conditions (3.1.23) through (3.1.26) as

$$\tau_e=\sum_{j=1}^{\infty}B_j\exp(-\mu_j\xi)S_j(\eta;C_j), \tag{3.2.10}$$

where the value of μ_j is determined from

$$\mu_j=\frac{\lambda_1}{2}\left(1+\frac{3}{2}L_D\frac{b_1^2}{\lambda_1^2}\right)\left\{-1+\sqrt{1+\frac{\frac{1}{3\pi}\left(\frac{32}{5}\right)^2\frac{1}{K_m^2}+b_1^2L_D+C_j^2}{\left\{\frac{\lambda_1}{2}\left(1+\frac{3}{2}L_D\frac{b_1^2}{\lambda_1^2}\right)\right\}^2}}\right\}. \tag{3.2.11}$$

The function $S_j(\eta;C_j)$ and the eigenvalue C_j are determined by solving Eq. (3.2.14), which will be derived in the following section. It is easily shown that the functions $S_1, S_2\cdots$ constitute a system of orthogonal functions under the orthogonal condition

$$\int_0^1\eta[J_0(b_1\eta)]^{1+\frac{3}{2}L_D}S_k(\eta)S_l(\eta)d\eta=0,$$

for $k\neq l$. The value of the coefficient B_j is obtained from

$$B_j=\frac{\int_0^1\eta[J_0(b_1\eta)]^{1+\frac{3}{2}L_D}S_j(\eta)\tau_0(\eta)d\eta}{\int_0^1\eta[J_0(b_1\eta)]^{1+\frac{3}{2}L_D}[S_j(\eta)]^2d\eta}. \tag{3.2.12}$$

The solution of the inhomogeneous equation (3.2.2) can be obtained from the solution of the homogeneous equation (3.2.8). However, the value of the inhomogeneous term including τ_a is very small in comparison with the other terms.

We neglect this term in the following argument. If we define $C_1<C_2<\cdots$, we obtain $\mu_1<\mu_2<\cdots$. For large ξ, we can approximately rewrite Eq. (3.2.10) as

$$\tau_e=B_1\exp(-\mu_1\xi)S_1(\eta;\ C_1),$$

as well as Eq. (3.2.3) for α. Even if the radial profile of the electron temperature is given in an arbitrary form at $\xi=0$, it is transformed into a function $S_1(\eta;\ C_1)$ far downstream of the origin. When we choose the initial profile of the electron temperature as

$$\tau_0(\eta)=S_1(\eta;\ C_1),$$

we obtain

$$\tau_e(\xi,\eta)=\exp(-\mu_1\xi)S_1(\eta;\ C_1). \tag{3.2.13}$$

In the expression of Eq. (3.2.13), μ_1 denotes the decay rate of the electron temperature along the tube axis.

3.2.3 *Determination of the Eigenfunction $S_j(\eta;\ C_j)$ and the Eigenvalue C_j*

The function $S_j(\eta;\ C_j)$ is the solution of the ordinary differential equation for $S(\eta)$

$$\frac{d^2S}{d\eta^2}+\left\{\frac{1}{\eta}+Z(\eta)\left(1+\frac{3}{2}L_D\right)\right\}\frac{dS}{d\eta}+[-L_D\{Z(\eta)\}^2+C^2]S=0, \tag{3.2.14}$$

with the boundary conditions

$$S(0)=1,\quad S(1);\ \text{finite}. \tag{3.2.15}$$

Equation (3.2.14) is derived from Eq. (3.2.8) by the method of separation of variables. The function $Z(\eta)$ diverges at $\eta=1$, because $J_0(b_1)=0$ as shown in Eq. (3.2.5). Therefore, both boundaries $\eta=0$ and $\eta=1$ are singular points. The elementary solutions of Eq. (3.2.14) are obtained in the form of series expansions as

$$S(\eta)=\begin{cases}1-\dfrac{1}{4}(C\eta)^2+\cdots\\ \left[1-\dfrac{1}{4}(C\eta)^2+\cdots\right]\log(C\eta)+\dfrac{1}{4}(C\eta)^2+\cdots,\end{cases} \tag{3.2.16}$$

in the vicinity of $\eta=0$, and

$$S(\eta)=(1-\eta)^{\gamma_+}\left\{1+\sum_1^\infty \tilde{s}_n^+(1-\eta)^n\right\}, \tag{3.2.17}$$

in the vicinity of $\eta=1$, where

$$\gamma_\pm=\frac{1}{2}\left\{-\frac{3}{2}L_D\pm\sqrt{\left(\frac{3}{2}L_D\right)^2+4L_D}\right\}, \tag{3.2.18}$$

$$\tilde{s}_n^{\pm}=\frac{\sum_{k=0}^{n-1}\{(\gamma_{\pm}+k)p_{n-k}-q_{n-k}\}\tilde{s}_k^{\pm}}{n(2\gamma_{\pm}-p_0+n-1)},$$

$$p_0=-1-\frac{3}{2}L_D, \qquad p_1=\frac{1}{2}-\frac{3}{4}L_D,$$

$$p_2=\frac{7}{12}+\frac{b_1^3}{3}+\left(-\frac{5}{8}+\frac{b_1^2}{2}\right)L_D, \qquad p_3=\frac{5}{8}-\frac{9}{16}L_D,$$

$$q_0=q_1=-L_D, \qquad q_2=-\left(\frac{13}{12}-\frac{2}{3}b_1^2\right)L_D+C^2,$$

$$q_3=-\left(\frac{7}{6}-\frac{b_1^3}{3}\right)L_D, \ \cdots.$$

With the conditions of Eq. (3.2.15), we obtain from Eqs. (3.2.16) and (3.2.17)

$$S(\eta)=S^{(0)}(\eta)\equiv 1-\frac{1}{4}(C\eta)^2+\cdots, \tag{3.2.19}$$

in the vicinity of $\eta=0$, and

$$S(\eta)=S^{(1)}(\eta)\equiv\tilde{s}_0(1-\eta)^{\gamma_+}\left\{1+\sum_1^{\infty}\tilde{s}_n^{+}(1-\eta)^n\right\}, \tag{3.2.20}$$

in the vicinity of $\eta=1$. The functions $S^{(0)}(\eta)$ and $S^{(1)}(\eta)$ constitute an analytic function by analytic continuation at an arbitrary point between $\eta=0$ and $\eta=1$.

In Eqs. (3.2.19) and (3.2.20), the coefficients C and $\tilde{s}_0$ are unknown. In principle, the values of C and $\tilde{s}_0$ can be determined by the matching conditions at an arbitrary point $\eta=\eta_1(0<\eta_1<1)$;

$$S^{(0)}(\eta_1)=S^{(1)}(\eta_1), \qquad \frac{dS^{(0)}(\eta_1)}{d\eta}=\frac{dS^{(1)}(\eta_1)}{d\eta}.$$

However, many terms are required to obtain $S^{(0)}(\eta)$ and $S^{(1)}(\eta)$ from Eqs. (3.2.19) and (3.2.20), so that the numerical calculation becomes rather complicated. Therefore, we use the following method of numerical calculation. For a prescribed value of C, we can obtain a curve for $S(\eta;C)$ through the numerical integration of Eq. (3.2.14), starting from the point $\eta=0$. The both values of the function $S(\eta;C)$ and its derivative are matched with the series solution (3.2.20) in the vicinity of $\eta=1$. As a matching condition, we use the relation

$$\frac{dS}{d\eta}=-S\left[\frac{\gamma_+}{1-\eta}+\frac{\sum_1^{\infty}n\tilde{s}_n^{+}(1-\eta)^n}{1+\sum_1^{\infty}\tilde{s}_n^{+}(1-\eta)^n}\right]. \tag{3.2.21}$$

Equation (3.2.21) is derived by eliminating $\tilde{s}_0$ from Eq. (3.2.20) and its derivative. Except appropriate values of C, the function $S(\eta;C)$ diverges as η approaches unity. The numerical integration of Eq. (3.2.14) is repeated untill Eq. (3.2.21)

holds in the vicinity of $\eta=1$ for a prescribed value of C. We obtain discrete values of C, for which Eq. (3.2.21) holds in the vicinity of $\eta=1$. These values are the eigenvalues $C_1, C_2, \cdots$. In other words, analytic continuation is possible only for these discrete values of C; $C_1, C_2, \cdots$.

In Eq. (3.2.17), two elementary solutions are possible for the value of γ; γ_+, γ_-. As seen from Eq. (3.2.18), one is positive and another negative. On the basis of the condition that the function $S(\eta)$ should be finite at $\eta=1$, the positive value γ_+ is chosen as shown in Eq. (3.2.20). From Eq. (3.2.20), we obtain

$$S(1)=0. \tag{3.2.22}$$

3.2.4 *Plasma Density and Electron Temperature Distributions in Poiseuille Flow*

In this section, we consider a fully developed viscous flow of neutral particles in contrast to the slug flow, for which the viscous effect is ignored. Only a laminar flow (Poiseuille flow) is analyzed, because the Reynolds number is small in the pressure range interested here. The normalized flow velocities $\bar{u}_a$ and $\bar{v}_a$ are given by

$$\bar{u}_a=2(1-\eta^2), \qquad \bar{v}_a=0, \tag{3.2.23}$$

when the mean flow velocity is chosen as a reference velocity U_0. Substituting Eq. (3.2.23) into Eqs. (3.2.1) and (3.2.2), and solving these equations with the boundary conditions (3.1.22) through (3.1.26) in the same way as in Sec. 3.2.2, we obtain the solutions for α and τ_e for large ξ as

$$\begin{aligned} \alpha&=\exp(-\bar{\lambda}_1\xi)Y_1(\eta;\bar{b}_1),\\ \tau_e&=\exp(-\bar{\mu}_1\xi)\bar{S}_1(\eta;\bar{C}_1). \end{aligned} \tag{3.2.24}$$

The functions $Y_1(\eta;\bar{b}_1)$ and $\bar{S}_1(\eta;\bar{C}_1)$ are the first eigenfunctions for the solutions of equations for $Y(\eta)$ and $S(\eta)$, respectively, as

$$\frac{d^2Y}{d\eta^2}+\frac{1}{\eta}\frac{dY}{d\eta}+(\bar{b}^2-2P_D\bar{\lambda}\eta^2)Y=0, \tag{3.2.25}$$

$$\begin{aligned} &\frac{d^2\bar{S}}{d\eta^2}+\left\{\frac{1}{\eta}+\bar{Z}(\eta)\left(1+\frac{3}{2}L_D\right)\right\}\frac{d\bar{S}}{d\eta}\\ &\quad+[\bar{C}^2-L_D\{\bar{Z}(\eta)\}^2-P_DL_D(3\bar{\mu}-2\bar{\lambda})\eta^2]\bar{S}=0, \end{aligned} \tag{3.2.26}$$

with the boundary conditions

$$Y(0)=1, \quad Y(1)=0; \qquad \bar{S}(0)=1, \quad \bar{S}(1);\ \text{finite},$$

where

$$\bar{\lambda}=P_D(-1+\sqrt{1+\bar{b}^2/P_D^2}), \tag{3.2.27}$$

$$\bar{Z}(\eta)\equiv\frac{1}{Y_1(\eta;\bar{b}_1)}\frac{dY_1(\eta;\bar{b}_1)}{d\eta}, \tag{3.2.28}$$

$$\beta=\frac{\bar{\lambda}_1}{2}\left(1+\frac{3}{2}L_D\frac{\bar{b}_1^2}{\bar{\lambda}_1^2}\right)\left[-1+\sqrt{1+\frac{\frac{1}{3\pi}\left(\frac{32}{5}\right)^2\frac{1}{K_m^2}+\bar{b}_1^2L_D+\bar{C}^2}{\left\{\frac{\bar{\lambda}_1}{2}\left(1+\frac{3}{2}L_D\frac{\bar{b}_1^2}{\bar{\lambda}_1^2}\right)\right\}^2}}\right]. \quad (3.2.29)$$

Equations (3.2.25) and (3.2.26) are solved in the same way as Eq. (3.2.14), and the eigenvalues $\bar{b}_1, \bar{b}_2, \cdots$ and $\bar{C}_1, \bar{C}_2, \cdots$ are obtained. It should be noted that the functions $Y_1, Y_2, \cdots$ and $\bar{S}_1, \bar{S}_2, \cdots$ do not constitute systems of the orthogonal functions except the cases of $P_D \to \infty$ and $P_D = 0$. Only the first functions Y_1 and $\bar{S}_1$ are presented as solutions for large ξ in Eq. (3.2.24).

3.3 Numerical Results and Discussion

3.3.1 *Numerical Examples of the Dimensionless Numbers P_D, K_m and L_D*

The numerical examples of the ambipolar Peclet number P_D and the modified Knudsen number K_m are tabulated in Tab. 3-1 for the case of $R=1$ cm, $p_a=1$ Torr, $T_e=5{,}000°K$, $T_a=300°$K and $U_0=100$ m/sec for argon, neon, helium and nitrogen. The values of P_D vary from 2 to 50 for these examples. For argon and neon, the larger values of K_m are obtained for the conditions prescribed here, because the effective hard sphere cross sections $Q_{ea}(T_e)$ for both gases are smaller than those of the other gases. The curves of $Q_{ea}(T_e)$ are shown in Fig. 3-2 for argon, helium, nitrogen and mercury vapour. These curves are obtained from Eq. (3.1.10) by using the data for the momentum transfer cross section for a monoenergetic beam of electrons in the reference [39]. In Fig. 3-3, the values of L_D are plotted against the electron temperature for these gases. The value of L_D varies from 10^{-5} to 10^{-2}.

TABLE 3-1. Examples of the values of R_e, P_D and K_m for $R=1$ cm, $p_a=1$ Torr, $T_a=300°$K, $T_e=5{,}000°$K and $U_0=100$ m/sec.

Gas	R_e	P_D	K_m
He	24	2.1	4.5
Ne	74	9.6	35
N_2	186	51	3.0
A	206	14	50

3.3.2 *Plasma Density*

As shown in Eqs. (3.2.7) and (3.2.24), the fully developed profile of the plasma density is expressed by the function $J_0(b_1\eta)$ for slug flow and by the function $Y_1(\eta; \bar{b}_1)$ for Poiseuille flow, respectively. The curves of $Y_1(\eta; \bar{b}_1)$ are shown in Fig. 3–4 for $P_D=0$, 1.0 and ∞. The curve for $P_D=0$ corresponds to the Bessel function $J_0(b_1\eta)$. The function $Y_1(\eta)$ does not deviate so much from the Bessel function $J_0(b_1\eta)$. The values of $\bar{b}_1$ are tabulated in Tab. 3–2 for several values of P_D.

In Fig. 3–5, the decay rates of the plasma density along the tube axis λ_1 and $\bar{\lambda}_1$ are plotted against P_D. Figure 3–5 is a graphical representation of Eqs. (3.2.4) and (3.2.27). The solid and broken lines correspond to slug and Poiseuille flows, respectively. The values of λ_1 and $\bar{\lambda}_1$ approach b_1 for $P_D \to 0$ and zero for $P_D \to \infty$.

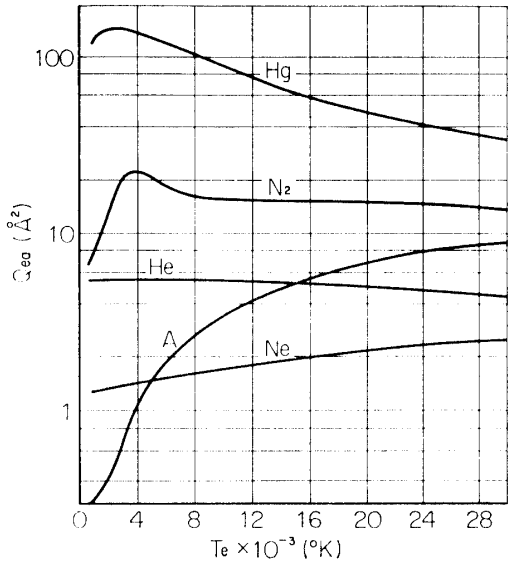

FIG. 3-2. Thermally averaged cross sections $Q_{ea}(T_e)$ for helium, neon, argon, nitrogen and mercury vapour.

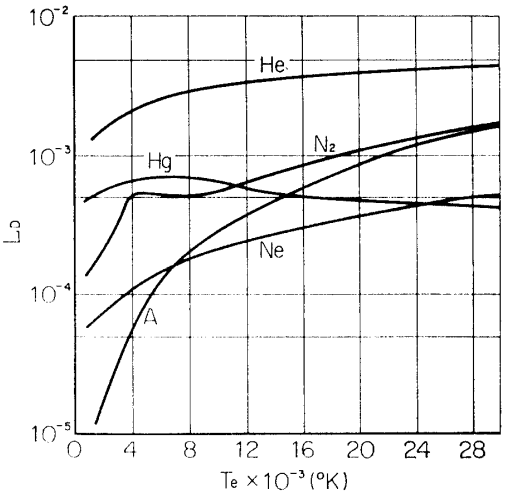

FIG. 3-3. Electron Lewis numbers L_D as a function of the electron temperature for helium, neon, argon, nitrogen and mercury vapour. The atom temperature is 480°K for mercury vapour and 300°K for the other gases.

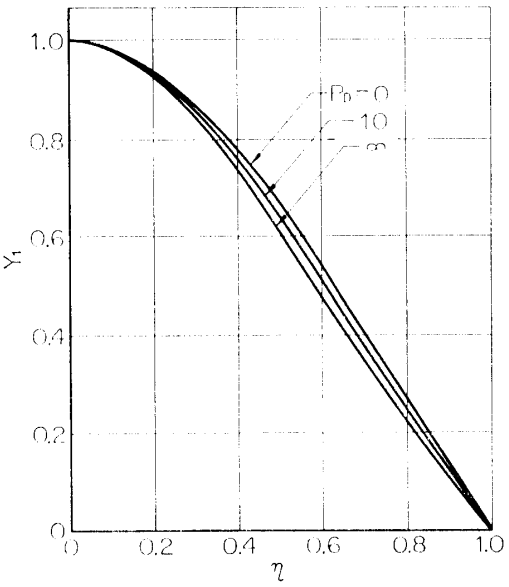

FIG. 3-4. Plasma density profiles in a circular tube at a great distance from the entrance for Poiseuille flow.

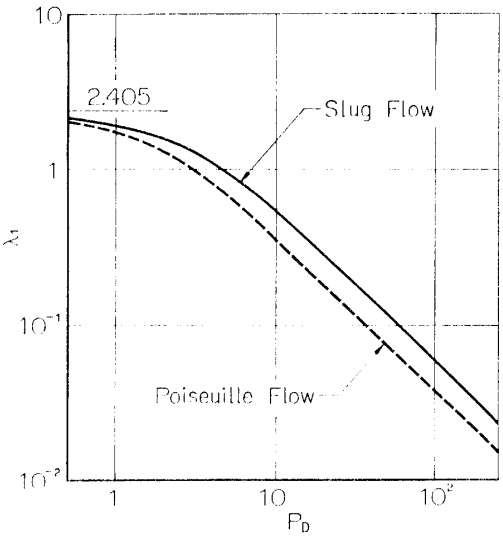

FIG. 3-5. Decay rates of the plasma density along the tube axis as a function of the ambipolar Peclet number P_D for slug and Poiseuille flows.

3.3.3 *The Eigenvalues and the Eigenfunctions for the Electron Energy Equations*

The eigenfunction C_j depends only on L_D. The values of C_1, C_2, C_3 and C_4 are tabulated in Tab. 3–3 for several values of L_D. The values of C_2, C_3 and C_4 are almost independent of L_D, while the value of C_1 depends on L_D. The eigenvalue

TABLE 3-2. The eiegnvalue $\bar{b}_1$.

P_D	$\bar{b}_1$	P_D	$\bar{b}_1$
0.0	2.4048	10.0	2.6984
0.1	2.4258	100.0	2.7034
1.0	2.5551	∞	2.7044
2.5	2.6428		

TABLE 3-3. The eigenvalues C_j (j=1, 2, 3, 4).

L_D	C_1	C_2	C_3	C_4
0.0	0.0	4.4086	7.6670	10.8590
0.00001	0.13501	4.4143	7.6723	10.8642
0.00002	0.16047	4.4167	—	—
0.00005	0.20159	4.4213	—	—
0.0001	0.23948	4.4266	7.6838	10.8754
0.0002	0.28436	4.4340	—	—
0.0005	0.35648	4.4486	—	—
0.001	0.42248	4.4650	7.7199	10.9108
0.002	0.49998	4.4880	—	—
0.005	0.62265	4.5329	—	—
0.01	0.73241	4.5825	7.8323	11.0215

$\bar{C}_j$ depends on L_D, P_D and K_m. The values of $\bar{C}_1$ are tabulated in Tab. 3–4 for several values of L_D, P_D and K_m. The value of $\bar{C}_1$ mainly depends on L_D, and does not deviate so much from the value of C_1 for the same value of L_D except the case of $K_m=0.1$.

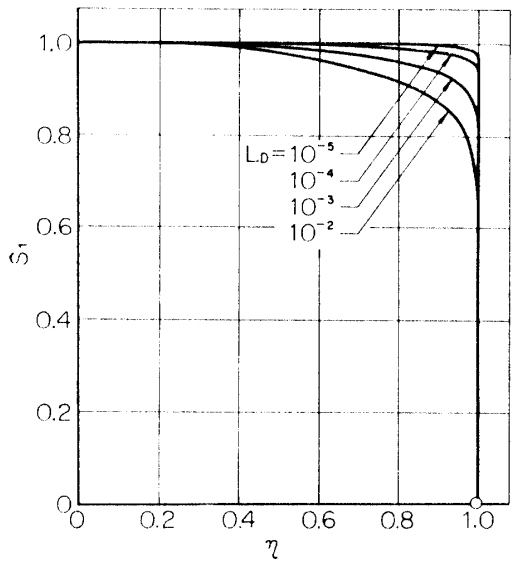

FIG. 3-6. Electron Temperature profiles in a circular tube at a great distance from the entrance. (slug flow)

As shown in Eqs. (3.2.13) and (3.2.24), the fully developed profile of the electron temperature is expressed by the function $S_1(\eta; C_1)$ for slug flow and by the function $\bar{S}_1(\eta; \bar{C}_1)$ for Poiseuille flow, respectively. The curves of the function $S_1(\eta)$ are shown in Fig. 3–6 for several values of L_D. The curves of $\bar{S}_1(\eta)$ do not deviate so much from the curves of $S_1(\eta)$ for the same value of L_D except the case of $K_m<1$. The electron temperature sharply decreases in the vicinity of $\eta=1$, and vanishes at $\eta=1$, while the radial gradient of the electron temperature is very small in the central part of the tube section. In actual phenomena, such a sharp change of the electron temperature is unexpected. Therefore, at first sight, the calculated

profiles of the electron temperature seem to be inconsistent with actual phenomena. However, it can be pointed out from the following argument that the solution for $S_1(\eta)$ is an unique solution which is consistent with physical situations in the neighborhood of the wall. Let us consider a fictitious wall at $\eta=\eta_\varepsilon=1-\varepsilon(\varepsilon\ll 1)$, and impose the condition that the electron temperature is finite at $\eta=\eta_\varepsilon$. From the physical point of view, the electron temperature is not very high in the neighborhood of the wall, so that we may assume that the order of the function $S_1(\eta)$ should be of unity. However, if the value of C exclusive of C_j is chosen, the function $S(\eta; C)$ diverges as η approaches unity. Only when the value of C is close to C_j, the function $S(\eta; C)$ has a moderate value of order one at the point $\eta=\eta_\varepsilon$, as far as ε is sufficiently small. Therefore, we may choose the function $S_1(\eta; C_1)$ as a function which is consistent with physical situations at $\eta=\eta_\varepsilon$. Equation (3.2.22) is regarded only as a mathematical condition.

TABLE 3-4. The eigenvalue $\bar{C}_1$ (P_D=0, 1, 10, 100).

L_D	K_m	P_D=0	1	10	100
10^{-5}	10^{-1}	0.13501	0.13210	0.13462	0.18615
	1		0.13147	0.12832	0.13448
	10		0.13142	0.12770	0.12829
	10^2		0.13142	0.12767	0.12789
	10^3		0.13142	0.12767	0.12788
10^{-4}	10^{-1}	0.23948	0.23690	0.26348	0.48288
	1		0.23335	0.23009	0.26324
	10		0.23309	0.22672	0.23151
	10^2		0.23308	0.22660	0.22999
	10^3		0.23308	0.22659	0.22999
10^{-3}	10^{-1}	0.42248	0.43195	0.58062	1.36483
	1		0.41252	0.41955	0.57543
	10		0.41112	0.40232	0.43476
	10^2		0.41110	0.40183	0.42999
	10^3		0.41110	0.40183	0.42994
10^{-2}	10^{-1}	0.73241	0.82029	1.44526	3.39432
	1		0.72009	0.79639	1.24756
	10		0.71306	0.72045	0.81872
	10^2		0.71295	0.71894	0.81073
	10^3		0.71295	0.71892	0.81065

3.3.4 *Decay Rates of the Electron Temperature along the Tube Axis*

Figures 3-7 (a) through (c) give graphical representations of Eqs. (3.2.11) and (3.2.29). The broken line in each figure corresponds to the limiting case of $P_D\to\infty$ and $L_D=0$, which is the case when the plasma density is constant throughout the flow field, and when the electron temperature distribution is quasi-one-dimensional along the tube axis. The solid and chain lines correspond to slug and Poiseuille

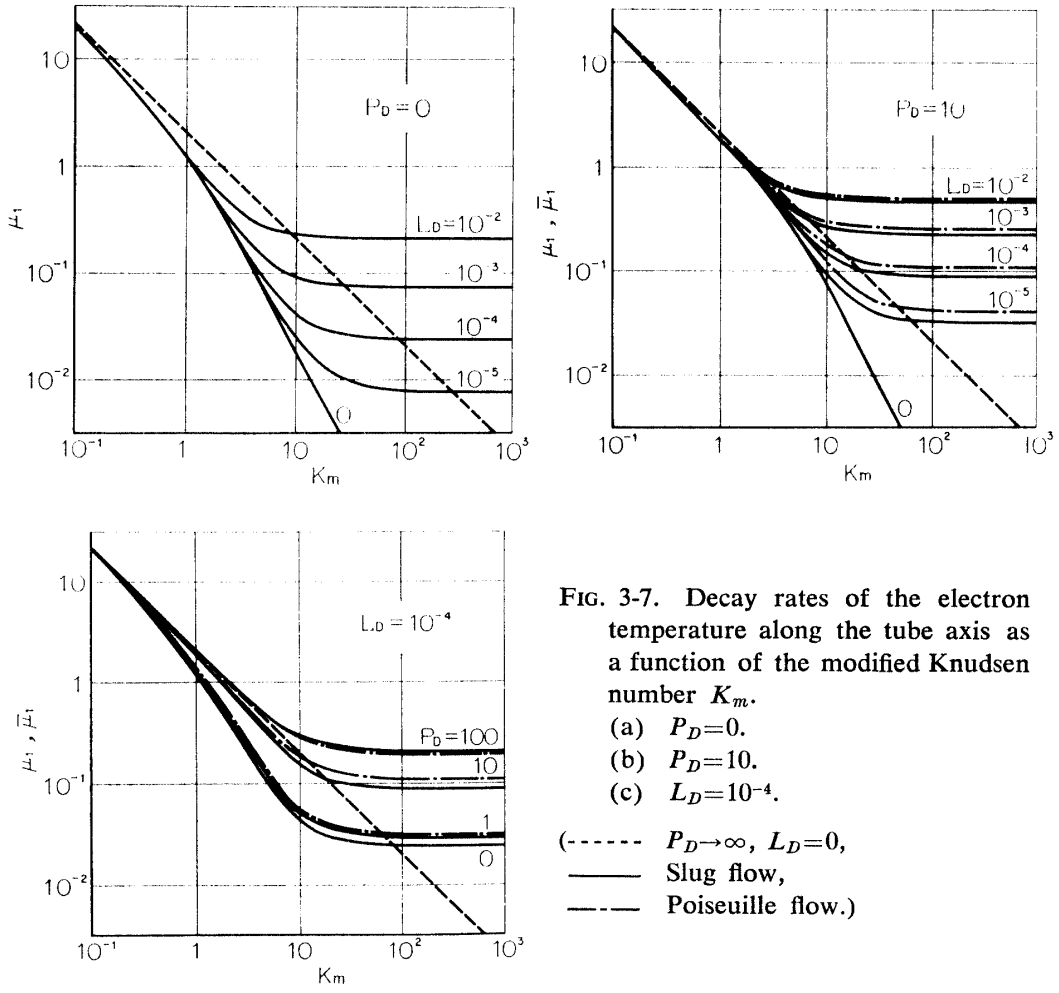

FIG. 3-7. Decay rates of the electron temperature along the tube axis as a function of the modified Knudsen number K_m.
(a) $P_D=0$.
(b) $P_D=10$.
(c) $L_D=10^{-4}$.
(------ $P_D\to\infty$, $L_D=0$,
——— Slug flow,
—·— Poiseuille flow.)

flows, respectively. The following results are obtained from Figs. 3-7 (a) through (c).

i) The decay rates of the electron temperature along the tube axis can be divided into three cases with respect to the modified Knudsen number K_m. For small K_m, the rates μ_1 and $\bar{\mu}_1$ mainly depend on K_m. On the other hand, for large K_m, these are independent of K_m, but depend on L_D and P_D. The boundary value of K_m for the former case is about 0.8 to 2.0, and that for the latter is about 20 to 100. In the case when the value of K_m is intermediate, the rates μ_1 and $\bar{\mu}_1$ depend on P_D, L_D and K_m.

ii) For small K_m, the decay rates increase as the value of K_m decreases. The case of small values of K_m is termed the collision-dominated case, since K_m is proportional to the mean free path of electron-atom collisions. The energy loss due to electron-atom collisions is predominant in the energy transfer processes of an electron gas. In the collision-dominated case, the values of μ_1 and $\bar{\mu}_1$ agree with the values for $L_D=0$. This agreement also denotes that the energy loss of electrons toward the wall is negligible in comparison with the energy loss due to collisions, because we obtain $S_1(\eta)=1$ for $L_D=0$. The difference between the values of μ_1 and $\bar{\mu}_1$ is undistinguishable.

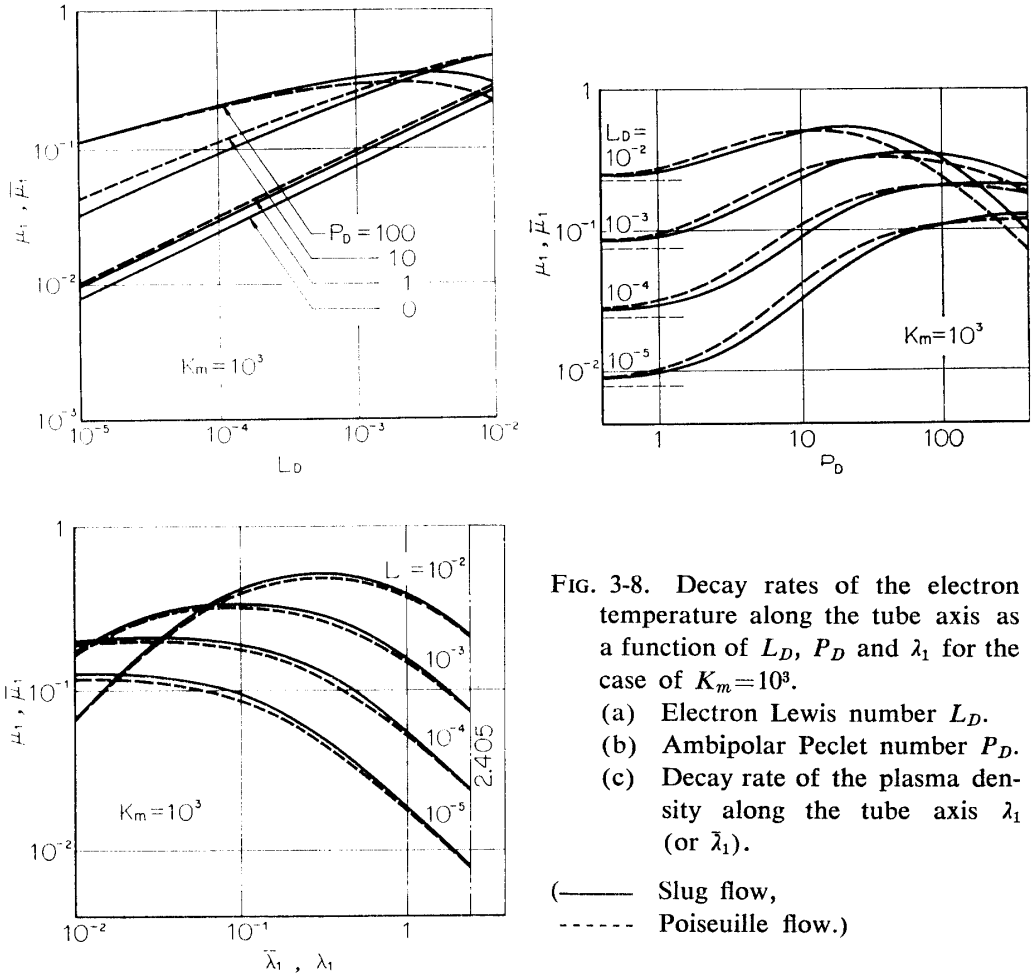

FIG. 3-8. Decay rates of the electron temperature along the tube axis as a function of L_D, P_D and λ_1 for the case of $K_m = 10^3$.
(a) Electron Lewis number L_D.
(b) Ambipolar Peclet number P_D.
(c) Decay rate of the plasma density along the tube axis λ_1 (or $\bar{\lambda}_1$).

(——— Slug flow,
------ Poiseuille flow.)

iii) The case of large K_m is termed the diffusion-dominated case, since P_D and L_D include the ambipolar diffusion coefficient. The energy transfer due to ambipolar diffusion and electron thermal conduction is predominant in the energy transfer processes of an electron gas. In the diffusion-dominated case, the values of μ_1 and $\bar{\mu}_1$ deviate from the values for $L_D = 0$, and mainly depend on P_D and L_D. The slight difference between the values of μ_1 and $\bar{\mu}_1$ can be recognized.

For the diffusion-dominated case, the values of μ_1 and $\bar{\mu}_1$ are plotted against L_D and P_D in Figs. 3-8 (a) and (b). The curves of μ_1 versus λ_1 and $\bar{\mu}_1$ versus $\bar{\lambda}_1$ are also shown in Fig. 3-8 (c). In the case when P_D is not so large, we obtain an approximate expression for μ_1 from Eq. (3.2.11) as

$$\mu_1 \sim C_1^2/\lambda_1, \tag{3.3.1}$$

for large K_m. Since C_1 increases with L_D as shown in Tab. 3-3, the rate μ_1 increases with L_D. When the eigenvalue C_1 is determined by solving Eq. (3.2.14) for $S(\eta)$, the fourth term of the left hand side of Eq. (3.2.14) $-L_D Z^2(\eta)-$ plays an important role. This term expresses the contribution of the electric field formed by ambipolar diffusion to the energy balance for electrons. The electrons diffusing

toward the wall lose their thermal energy across the negative potential barrier. Therefore, C_1^2 appearing in Eq. (3.3.1) expresses the contribution of energy loss of electrons toward the wall to the rate μ_1. The rate λ_1 of the right hand side of Eq. (3.3.1) is derived from the thermal conductivity, which is proportional to the plasma density. That is, the variation of the electron thermal conductivity with the plasma density contributes to the value of the decay rate μ_1. When the value of λ_1 approaches zero (P_D increases), we obtain an approximate expression for μ_1 as

$$\mu_1 \sim \lambda_1 C_1^2 / L_D,$$

instead of Eq. (3.3.1). The rate μ_1 decreases as P_D increases, in contrast to Eq. (3.3.1). As L_D increases, the decrease of the rate μ_1 with λ_1 appears for the smaller values of P_D; e.g., the curves for $P_D=100$ in Fig. 3-8 (a) and for $L_D=10^{-2}$ in Figs. 3-8 (b) and (c). In the case of large P_D, the contribution of the variation of the electron thermal conductivity becomes small, and the convective and diffusive transfer of electron energy along the tube axis becomes predominant.

3.4 Quasi-One-Dimensional Approximation

In this section, the energy loss of electrons toward the wall is neglected. The electron temperature is assumed to be constant in each section of a circular tube. The radial gradients of α and τ_e in the energy equation (3.2.2) are neglected. The rates μ_1 and $\bar{\mu}_1$ for the quasi-one-dimensional approximation are obtained by assuming $C_1=0$ and $\bar{C}_1=0$ in Eqs. (3.2.11) and (3.2.29), respectively.

As an example, the curves of μ_1 versus K_m are shown in Fig. 3-9 for the case of $P_D=10$. In the collision-dominated case, the curves agree with those obtained from the preceding analysis for an axially symmetric flow. This agreement implies that the quasi-one-dimensional approximation can be applied to the collision-dominated case. In the diffusion-dominated case, the values of μ_1 are smaller by one orde or two orders of magnitude than those obtained from the preceding analysis, because the electrons lose their energies only by the action of thee lectric field formed by the plasma density gradient along the tube axis for the case of quasi-one-dimensional approximation.

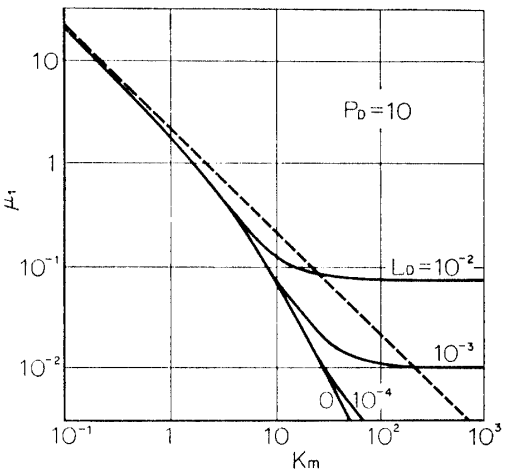

FIG. 3-9. Decay rates of the electron temperature along the tube axis for quasi-one-dimensional approximation.

(------ $P_D\to\infty$, $L_D=0$.)

IV. An Example of the Measured Decay Rates of the Electron Temperature along a Tube Axis

In the present chapter, we compare the calculated decay rates of the electron temperature along the tube axis with the rates measured by Konenko [28] in a diffusion flow of stationary helium plasma. The experimental conditions correspond to the collision-dominated case (for small K_m). A glass tube with oxide cathode was used. The spiral anode divides the tube into two parts. One is the ionization region, and the other the diffusion region. In the ionization region, a discharge is excited. From the positive column of this region, plasma diffuses through the anode into the other side of the tube, containing a mobile Langmuir probe. The electron temperature curves along the tube axis were taken for the pressure range from 0.6 to 4 Torr. The plasma density and the electron temperature at the anode are about $4\sim5\times10^{8}/\mathrm{cm}^3$ and 3×10^{4} °K, respectively. The gas temperature is considered to be room temperature. The estimated value of L_D is equal to 5×10^{-3}. The value of K_m varies from 0.4 to 3. The corresponding value of K_n varies from 2.3×10^{-3} to 1.8×10^{-2}.

The electron temperature distribution was expressed by the semi-empirical formula

$$T_e=T_\infty \exp[k' \exp(-\gamma' x)].$$

The values of the maximum electron temperature gradient $k'\gamma'$ have been obtained from the electron temperature curves through the relation

$$k'\gamma'=-\left.\frac{d\ln T_e}{dx}\right|_{x=0}, \qquad (4.1)$$

and plotted against helium pressure. In the present analysis, the relative electron temperature gradient can be expressed as

$$\frac{d\ln T_e}{dx}=-\mu_1/R. \qquad (4.2)$$

By comparing Eq. (4.2) with Eq. (4.1), we obtain the relation

$$\mu_1=k'\gamma'R. \qquad (4.3)$$

We can obtain the value of μ_1 from the measured value of $k'\gamma'$ through Eq. (4.3). The values of μ_1 thus obtained are plotted against K_m in Fig. 4-1. The solid lines correspond to the case

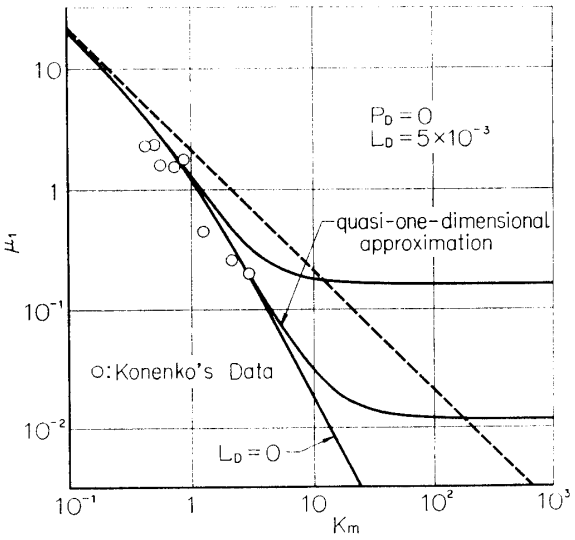

FIG. 4-1. Comparison of measured and calculated decay rates of the electron temperature along the tube axis for the collision-dominated case.

(------ $P_D\to\infty$, $L_D=0$.)

of $L_D=0$ and 5×10^{-3} for $P_D=0$. The curve for quasi-one-dimensional approximation is also shown in the figure. The broken line corresponds to the limiting case of $P_D\to\infty$ and $L_D=0$. The measured values of μ_1 are found to be in qualitative agreement with the values obtained from the present analysis. The measured rates increase as the value of K_m decreases, and agree with the estimated rates in the order of magnitude.

V. Experimental Study of a Pipe Flow of Weakly Ionized Nonequilibrium Argon

5.1 Experimental Apparatus

A schematic diagram of the experimental apparatus is shown in Fig. 5-1. The apparatus mainly consists of the high pressure bottle for gas supply, the discharge chamber, the circular tube, the test section, the vacuum tank (5 m^3) and the vacuum pumps; a mechanical booster (2,000 m^3/h) and a oil rotary pump (3 m^3/min). The test gas is supplied from the high pressure bottle into the discharge chamber, and ejected into the test section through the circular tube. The test gas is ionized by dc glow discharge between ring electrodes mounted at both ends of the discharge chamber.

The discharge chamber and the test section are made of steel cylinder of 130 mm in inner diameter and 300 mm in length. The outside view of the discharge chamber and the test section is shown in Fig. 5-2. A schematic diagram of the discharge chamber is shown in Fig. 5-3. Both electrodes are ring-like and 60 mm in inner diameter. The anode and the cathode are 2 mm and 30 mm in length, respectively, and made of steel. The cathode is a cold one. The test gas is injected into the discharge chamber through holes drilled on the hemisphere of a ping-pong

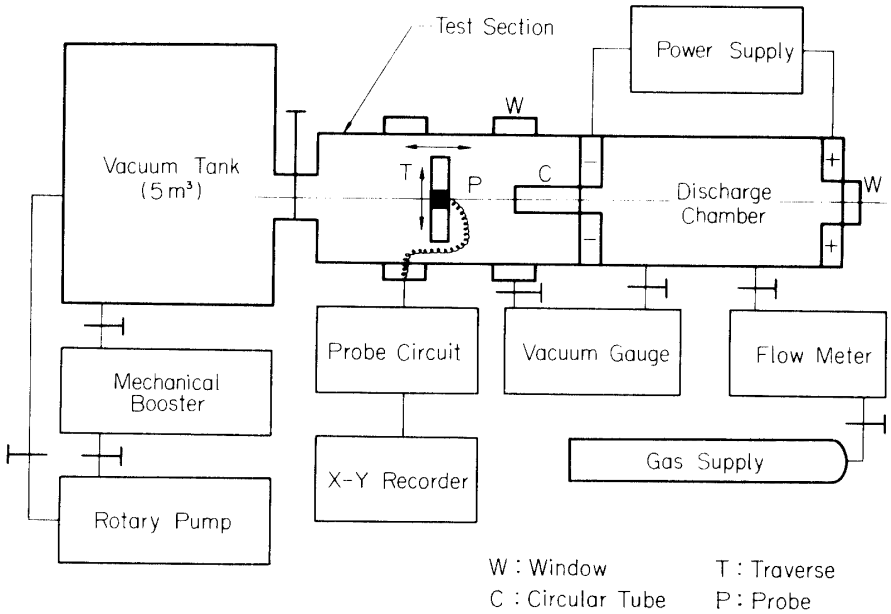

FIG. 5-1. A schematic diagram of the experimental apparatus.

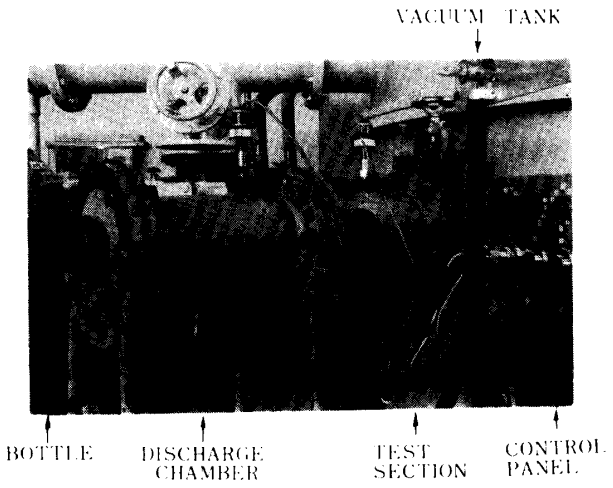

FIG. 5-2. The outside view of the discharge chamber and the test section.

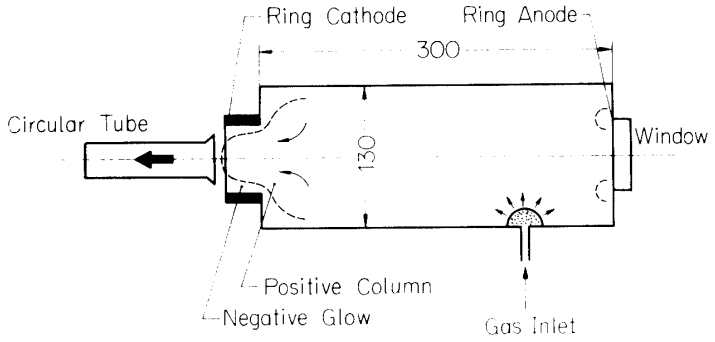

FIG. 5-3. A schematic diagram of the discharge chamber.

ball fixed on the chamber wall, and runs through the ring cathode into the circular tube. It is observed from the window that the test gas at the center of the ring cathode has luminescence of the positive column of argon plasma, and that it is surrounded by ring-like negative glow. It is estimated that the positive column projects into the cathode ring as shown in Fig. 5-3. The circular tubes of 20.4 mm and 37.5 mm in inner diameter, and 80 mm in length are employed. Since the diameter of the cathode ring is 60 mm, it is estimated that the central core of the plasma in the ring flows down through the tube. In fact, the plasma potential measured in the tube is nearly equal to the potential of the positive column.

When polarity of the ring electrodes is exchanged, the plasma density measured in the tube becomes about one tenth to one hundredth less than that for the former polarity of the electrodes. As the plasma density decreases, the assumption of quasi-neutrality becomes invalid. As will be shown later in Sec. 5.4.2, the assumption of quasi-neutrality is valid, when the polarity of the electrodes is chosen as shown in Fig. 5-3. Furthermore, trial use is made of the spiral cathode or spiral anode as used by Konenko [*28*]. In the case of the spiral electrode, the electric

probes, which are used to determine the electron temperature and the plasma density, becomes rapidly dirty, so that the measured electron temperature becomes uncertain. Therefore, we employ the method of discharge as shown in Fig. 5-3.

5.2 Method of Measurements

The mean flow velocity in the circular tube is determined from the volume flow rate, which is measured by the flowmeter, as $u_m = Q_0/\pi R^2$, where u_m is the mean flow velocity and Q_0 the volume flow rate. Moreover, a pitot tube with flat nose (3 mm in diameter) is used to determine the radial distribution of the flow velocity in the section of the tube exit. The pitot pressure is measured by the Pirani-gauge.

The electron temperature is measured by the double probe. The equivalent resistance method, which has been proposed by Johnson and Malter [*44*], is used to determine the electron temperature from the voltage-current curve. We use the cylindrical probes made of tungsten or molybdenum. The probes are 3 mm in length and 0.1 or 0.2 mm in diameter. The distance between two elements of the probe is about 2.5 mm. The probe is placed in parallel with the tube axis, and moved in directions parallel and normal to the axis. The X-Y recorder is used to obtain the voltage-current curve.

In the present experiment, we need the axial and radial profiles of the plasma density in a circular tube, but the precise value of the plasma density is not necessary, so that we may use the method of Malter and Webster [*45*] to determine the plasma density. Moreover, in order to determine the radial profile of the plasma density, a single probe with strongly negative bias is employed instead of the double probe, which is inferior to the single probe with respect to space resolution. The radial profile of the ion current is utilized to gain the information about the radial profile of the plasma density. Initially, the floating potential is measured at a few points in the circular tube. Then, the probe potential is fixed at the potential which is nearly equal to -10 volts relative to the floating potentials, and the probe is moved in the radial direction in a constant speed by using the servomotor. The radial profile of the ion current is plotted by the recorder.

5.3 Experimental Results and Discussion

5.3.1 *Flow Velocity*

The experiment is carried out for the case of the chamber pressure of 0.5, 1 and 2 Torr. The test gas is argon. The chamber pressure is adjusted by the needle valve of the flowmeter. The mean flow velocity is controlled by adjusting the opening of the valve between the vacuum tank and the rotary pump. The pipe flow with the mean velocities between 30 and 120 m/sec is obtained.

The radial distribution of the flow velocity at the tube exit is shown in Fig. 5-4 for the case of chamber pressure of 1 Torr. The flow velocity on the axis of the tube is about 200 m/sec, which corresponds to the Mach number of 0.6. The change of the sound velocity is estimated within 5%, so that the Mach number distribution measured by the pitot tube can be considered as a velocity distribution. In Fig. 5-4, the measured velocity distribution nearly agrees with a Poiseuille distribution.

Similar results are obtained for the chamber pressures of 0.5 and 2 Torr.

In the case of Fig. 5-4, the estimated initial length is about 20 cm. Since the tube length is 8 cm, the tube exit corresponds to half of the initial length. The calculated distribution at half of the initial length nearly agrees with a parabolic distribution [*46*], and cannot be distinguished from a Poiseuille distribution within the present experimental accuracy. At the other section of the tube, it is not assured that the velocity distribution nearly agrees with a Poiseuille distribution. However, the detailed measurements of the velocity distribution are not carried out, because it is estimated that the plasma density and the electron temperature distributions are not affected by velocity profiles so much.

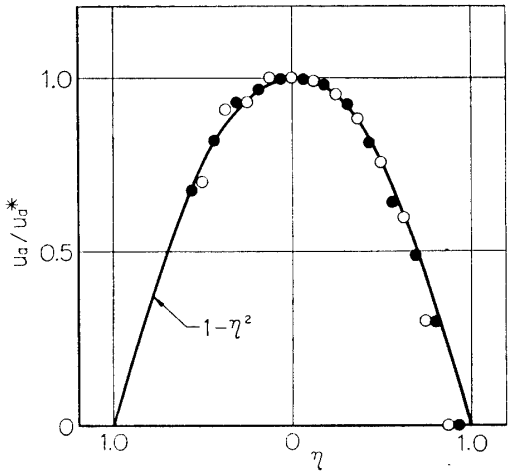

FIG. 5-4. Comparison of measured and calculated velocity profiles at the tube exit. The discharge chamber pressure is 1 Torr. The mean flow velocity is 103 m/sec.

5.3.2 *Discharge*

The discharge current applied is 0.1 to 0.15 A and the discharge voltage 400 to 500 V. The variations of the discharge current and voltage remain within 2~3%, or sometimes within 5%. Stable discharge is confirmed by observing the glow of discharge from the window of the end plate of the discharge chamber. The intensity of photo-emission of the glow is observed by the photomultiplier. The variation of its outputs is recorded by the syncroscope, and is found to remain within 0.5% even in the case of the largest fluctuation of the intensity for the case of the chamber pressure of 2 Torr.

5.3.3 *Plasma Density and Electron Temperature*

The radial distributions of the ion current at five sections of the circular tube of 2.04 cm in diameter are shown in Fig. 5-5 for the case of the discharge chamber pressure of 1 Torr. The center of the middle section between the inlet and the exit is chosen as a reference point. At the tube inlet ($\xi=-4$), the radial distributions of the ion current are found to be various forms immediately upstream of the inlet, but these immediately approach a similar profile. At $\xi=-2$, the ion current profile nearly coincides with the calculated radial profile $J_0(b_1\eta)$ of the plama density. At the other sections, similar results are obtained. Therefore, we can apply the present analysis to the flow for $\xi\geq-2$.

The radial distribution of the electron temperature is measured by the double probe, and shown in Fig. 5-6. The radial distribution of the plasma density which is measured by the double probe, is also shown in Fig. 5-6. The electron tempera-

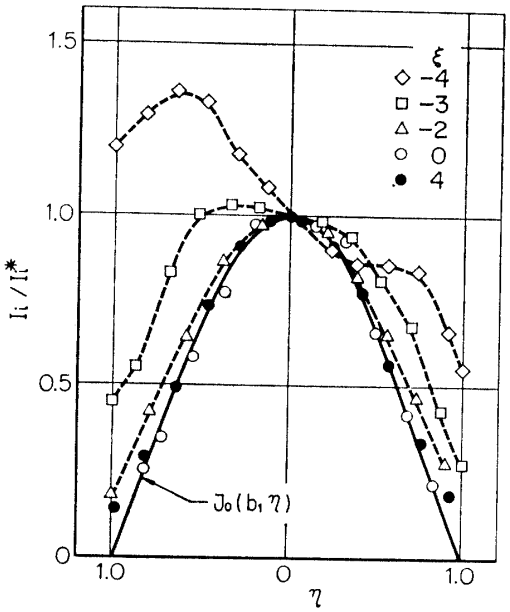

FIG. 5-5. Radial distributions of the ion current at several tube sections, where $\xi=4$ corresponds to the tube exit. The discharge chamber pressure is 1 Torr.

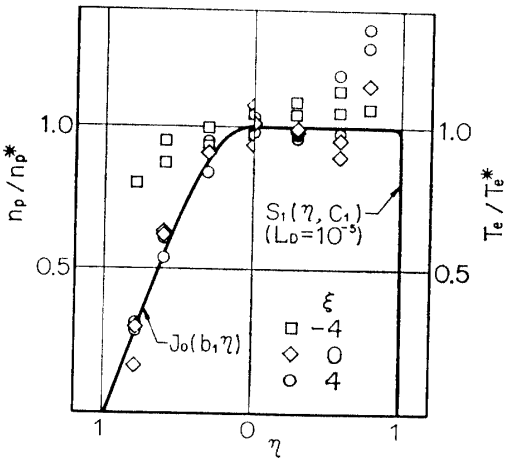

FIG. 5-6. Comparison of measured and calculated profiles of the plasma density and the electron temperature at a few sections.

ture is nearly constant within scattering of $\pm 10\%$ around the axis, but increases toward the wall. This increase of the measured values of the electron temperature is estimated to be caused by the double-probe characteristic, which is affected by the space field near by the wall.

The axial distributions of the plasma density and the electron temperature are shown in Fig. 5-7 in the form of semi-log plots. The straight lines can be drawn to determine the values of μ_1 and λ_1. These values are obtained by the method of least squares. The standard deviations are below 0.05 for all data. At the reference point ($\xi=0$), the measured electron temperature varies from 4,000°K to 5,000°K, and the measured plasma density varies from 5×10^{9} to $5\times10^{11}/\text{cm}^3$. The values of P_D, L_D and K_m evaluated at the reference point are 5 to 30, 6×10^{-5} to 9×10^{-5} and 30 to 140, respectively. In the evaluation of the values of K_m, the atom number density is assumed to be the mean of the densities of the discharge chamber and the test section.

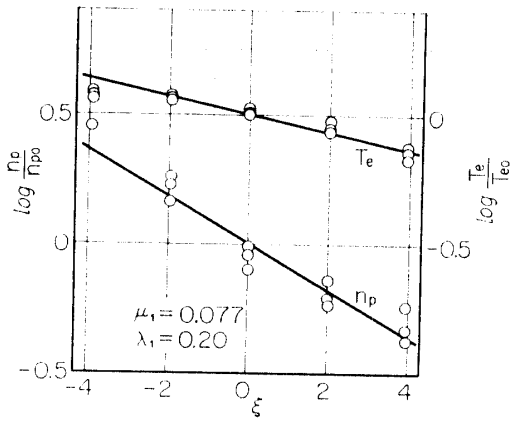

FIG. 5-7. Typical log-plots used to obtain the decay rates of the plasma density and the electron temperature along the tube axis.

In Fig. 5-8(a), the measured values of λ_1 are plotted against P_D. The solid and broken lines are the theoretical curves for slug and Poiseuille flows, respectively.

It is found that the measured decay rates of the plasma density nearly agree with the rates evaluated from the analysis. In Fig. 5-8(b), the measured values of μ_1 are plotted against K_n, the ordinary Knudsen number which is defined by the ratio of the electron mean free path to the tube diameter. The decay rates of the electron temperature along the tube axis are measured between $K_n=0.06$ and 0.3 or $K_m=30$ and 140. The solid and chain lines are the curves evaluated, respectively, from the axially symmetric analysis and from the quasi-one-dimensional approximation for slug flow for the case of $L_D=5\times10^{-5}$, $P_D=5$ and 50. The broken line corresponds to the case of $L_D=0$ and $P_D\to\infty$. It is found from Fig. 5-8(b) that the order of magnitude of the measured decay rates agrees with that of the rates evaluated from the axially symmetric analysis, and that the values of the measured rates increase with P_D independently of K_n or K_m. In Figs. 5-8(c) and (d), the

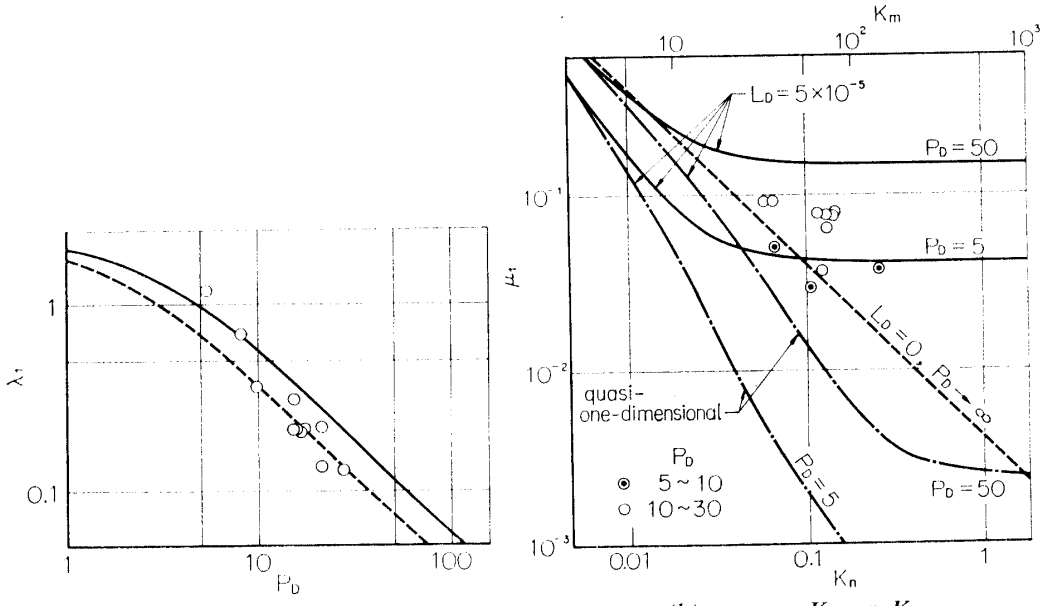

(a) μ_1 vs. P_D. (b) μ_1 vs. K_n or K_m.

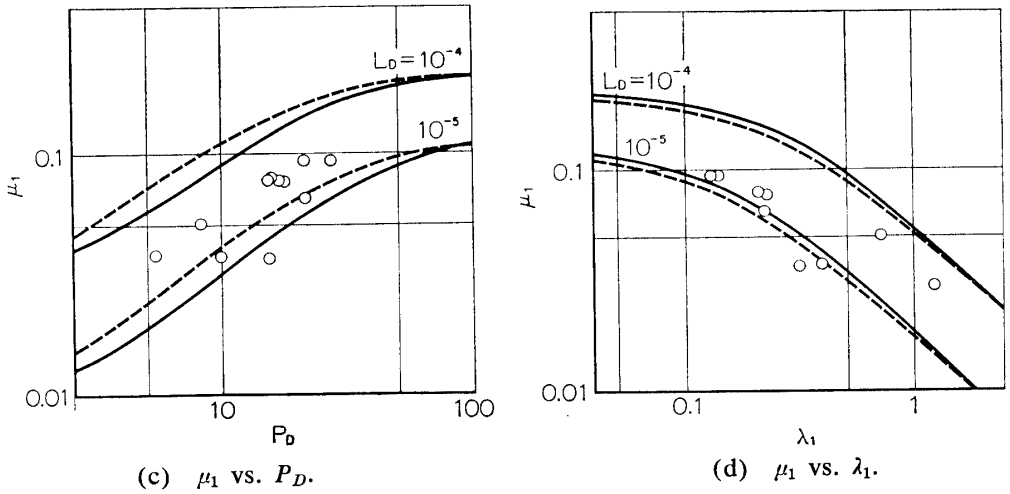

(c) μ_1 vs. P_D. (d) μ_1 vs. λ_1.

FIG. 5-8. Experimental results.

measured values of μ_1 are plotted against P_D and the measured values of λ_1, respectively. The theoretical curves are also shown for $L_D=10^{-5}$ and 10^{-4} for the case of $K_m=10^3$. The solid and broken lines correspond to slug and Poiseuille flows, respectively. Figures 5-8(c) and (d) show that the measured decay rates of the electron temperature qualitatively agree with the rates evaluated from the present analysis. The measured rates increase as P_D increases.

5.3.4 *Floating Potential*

The floating potential distributions are measured along the tube axis for a few cases. In Fig. 5-9, the measured values of the normalized floating potential gradient at the reference point $(d\bar{\phi}_f/d\xi)_{\xi=0}$ are plotted against P_D, where we define $\bar{\phi}_f=e\phi_f/(kT_{e0})$. The solid and broken lines show the curves of $(d\bar{\phi}_f/d\xi)_{\xi=0}$ versus P_D, evaluated from the present analysis for slug and Poiseuille flows, respectively. The signs of both estimated and measured gradients of the floating potential become positive as P_D increases. The absolute value of the measured gradient of the floating potential is not so accurate, because the fluctuation of the floating potential is large. However, the reversal of the sign of the gradient is clearly obtained. According to the present analysis, this reversal of the sign is caused by the increase of the electron temperature gradient with P_D.

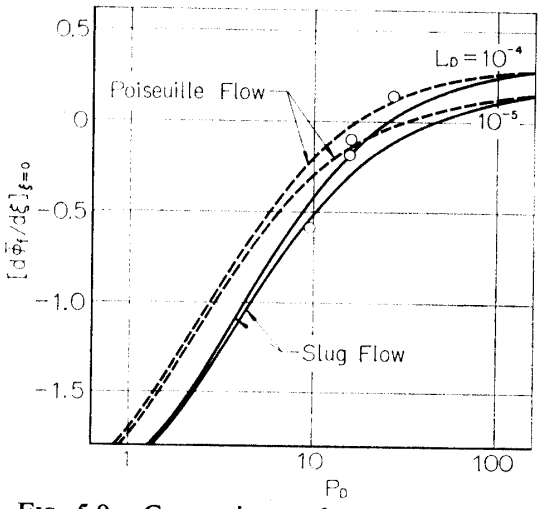

FIG. 5-9. Comparison of measured and calculated gradients of the floating potential along the tube axis.

Therefore, this experimental result seems indirectly to support the analytical result for the electron temperature distribution along the tube axis.

5.4 *Examination of the Experimental Conditions*

5.4.1 *Impurities*

If the particles with large cross section for electron-atom collisions are mixed in the test gas, the effective cross section for the mixture becomes larger than the cross section for the test gas. The value of the cross section affects the estimated values of L_D and K_m. In the present section, the degree of impurity level is estimated.

The particles with the largest cross section for electron-atom collisions are alkali-metals. The cross sections between electrons and alkali-atoms are about thousand times larger than the cross section between electrons and argon-atoms [*39*]. If the effective cross section for the mixture is larger by one order of magnitude than the cross section for argon, the effects of impurities become predominant. When the alkali-vapour is above 0.1% in the argon gas, the effective cross section for the mixture exceeds the cross section for electron-argon atom collisions. This impurity

level is considered uncommon. The gas which is estimated to be mixed, is air. The cross section between electrons and nitrogen or oxygen molecules is about thirty times larger than that for argon. The measured rate of volume flow of air leakage is about 0.1% of the rate of volume flow of argon. The contribution of the air molecules to the total cross section is estimated to be below a few percent.

5.4.2 *Assumption of the Analysis*

The analysis of Chap. III is based on the assumptions quoted in Sec. 3.1.1. In the present section, we inquire whether the experimental conditions satisfy these assumptions. Rough criterions are given with respect to the regions of the electron number density n_e, the electron temperature T_e and the gas pressure p_a.

a) Quasi-neutrality: As a criterion, we assme $\lambda_D^*/R<0.02$, where λ_D^* is the Debye length at the tube axis.

b) Weakly ionized: As a criterion, we assume $n_a Q_{ea}<n_e Q_{ee}$, where Q_{ee} is the cross section for electron-electron collisions.

c) Frozen recombination: As a criterion, we assume the condition that the loss of the charged particles resulting from ambipolar diffusion overcomes the loss resulting from recombination in the gas phase. Stationary decaying plasma in an infinite cylinder is considered. By comparing the time when the electron number density becomes equal to $n_0 \exp(-1)$, we obtain the criterion,

$$n_0<\frac{\exp(1)-1}{\alpha_r}\frac{b_1^2 D_a}{R},$$

where n_0 is the electron number density at $t=0$, α_r recombination coefficient. Most of the measured values of α_r has been obtained at $T_e=300°\mathrm{K}$ for afterglow plasmas, in which dissociation recombination is predominant. The recombination coefficients of molecular-rare-gas ions (helium, neon, argon, krypton and xenon), which have been measured by several authors, are tabulated in reference [*47*]. For high electron temperature, it has been found that the recombination coefficient α_r for dissociation recombination is proportional to $T_e^{-3/2}$, experimentally [*48*] and theoretically [*49*].

d) Frozen ionization: As a criterion, we assume the condition that the loss of the charged particles resulting from ambipolar diffusion overcomes the production of the charged particles resulting from the impact of high energy electrons with atoms. This criterion may be given from Schottky's diffusion theory for stationary plasmas in a discharge tube.

e) High electron temperature: As a criterion, we assume $T_e/T_a>5$.

f) Short mean free paths for ions and atoms: The mean free paths for ions and atoms are assumed to be much smaller than the tube diameter. The significance of this assumption will be discussed in the following section. As a criterion, we assume $l_{aa}/R<0.05$, where l_{aa} is the mean free path for atom-atom collisions. The criterion for ion mean free path is not assumed, since its order of magnitude nearly agrees with that of atoms.

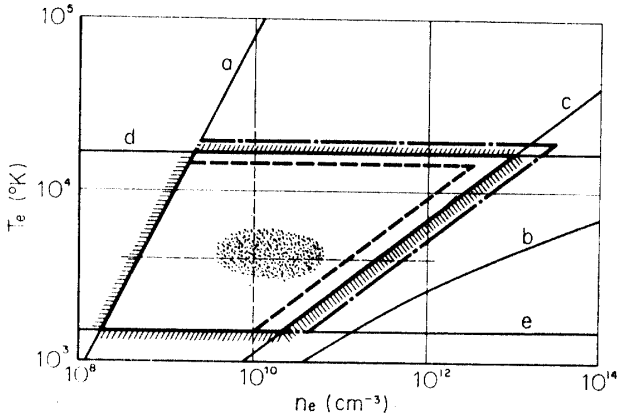

FIG. 5-10. Regime for applicability of the assumptions of the present analysis for argon, $R=1$ cm, and $T_a=300°K$. T_e-n_e plane (——— $p_a=1$ Torr; ------ 2 Torr; —·— 0.5 Torr).

On the basis of the criterions a) through f), the regime for applicability of the assumptions can be expressed as a space region in the space coordinates n_e, T_e and p_a, if the gas species, the tube radius and the atom temperature are given. An example of the regime for applicability of the assumptions is illustrated for argon, $R=1$ cm and $T_a=300°K$. For convenience, the cut plane is presented. The plane T_e-n_e is shown in Fig. 5-10 for the case of $p_a=1$ Torr. The lines ***a*** to ***e*** correspond to the criterions a) to e), respectively. The value of α_r is assumed to be the largest value already measured; $\alpha_r \sim 10^{-6}$ cm^2/sec [*47*] at $T_e=300°K$. The boundaries of the regime for applicability are expressed by hatching. For comparison, the boundaries for the cases of $p_a=0.5$ and 2 Torr are also shown by chain and broken lines, respectively. The region expressed by dotted points corresponds to the region studied in the present experiment. The present experimental conditions are found to satisfy the criterions a) through e).

5.4.3 *Mean Free Path*

As quoted in the preceding section, the mean free paths for ions and atoms are much smaller than the tube diameter. On the contrary, as shown in Fig. 5-8(b), the experiment is carried out for the ordinary Knudsen number around 0.1 for electron-atom collisions. The electron mean free path is not much smaller than the tube diameter. As for the plasma density, the continuum condition is satisfied, because ambipolar diffusion is controlled by the ion-atom collisions and the space field regardless of the electron-atom collisions. As for the electron temperature, the electron thermal conductivity cannot always be used for the case of large Knudsen number for electrons. However, it is expected that the continuum approach can be applied as an analytical model, when the Knudsen number is not so large (below unity) as in the present case.

VI. Conclusions

In the present paper, some characteristics of the energy transfer processes of an electron gas at low density are clarified by solving the energy equation for electrons for a pipe flow of weakly ionized nonequilibrium plasmas and by comparing the analytical results with the experimental results. The electron temperature distribution in a circular tube is analytically obtained, and compared with the measured distribution.

The results are summarized as:

1) It is found from the dimensional analysis of the energy equation for electrons that the electron temperature distribution in the flow depends on the dimensionless numbers P_D, L_D and K_m which are termed the ambipolar Peclet number, the electron Lewis number and the modified Knudsen number, respectively, defined by Eqs. (3.1.20) through (3.1.22).

2) It follows from the analysis that the electron temperature exponentially decreases along the tube axis. The decay rates of the electron temperature along the tube axis are obtained in analytical formulae given by Eqs. (3.2.11) and (3.2.29), respectively, for both slug and Poiseuille flows.

3) The decay rates are mainly divided into three cases with respect to the modified Knudsen number K_m. For small K_m, the decay rates mainly depend on K_m, while for large K_m the rates depend on the ambipolar Peclet number P_D and the electron Lewis number L_D. The boundary value of K_m for the former case is about 0.8 to 2.0, and that for the latter is about 20 to 100. For the intermediate values of K_m, the decay rates depend on K_m, L_D and P_D.

4) For small K_m the decay rates increase as the value of K_m decreases. The case of small value of K_m is termed the collision-dominated case, since the energy loss due to electron-atom collisions is predominant in the energy transfer processes of an electron gas.

5) For large K_m, the decay rates increase as the value of L_D or P_D increases, unless P_D is very large. The case of the large value of K_m is termed the diffusion-dominated case, since the electron energy transfer due to ambipolar diffusion and electron thermal conduction is predominant in the energy transfer processes of an electron gas. It is pointed out that the dependence of the rates on P_D is mainly caused by the variation of the electron thermal conductivity with the plasma density.

6) It follows from the simple analysis of the quasi-one-dimensional approximation of the energy equation for electrons that in the collision-dominated case the decay rates are very close to the rates evaluated from the simple analysis. Therefore, in this case the quasi-one-dimensional approximation may be applied to the present problem. On the contrary, in the diffusion-dominated case the decay rates deviate from the rates estimated from the simple analysis.

7) As for the collision-dominated case, the decay rates measured by Konenko [*28*] for a diffusion flow of stationary helium plasma are found to be in qualitative agreement with the rates from the present analysis. The measured rates increase as the value of K_m decreases, and agree with the estimated rates in the

order of magnitude. This data may be considered to support the analysis in part for the collision-dominated case.

8) As for the diffusion-dominated case, the decay rates are measured for a pipe flow of weakly ionized nonequilibrium argon. The value of the modified Knudsen number varies from 30 to 140, and corresponds to the value of the ordinary Knudsen number of 0.06 to 0.3. The measured decay rates are also found to be in qualitative agreement with the rates evaluated from the present analysis. The measured rates increase as the ambipolar Peclet number P_D increases, and agree with the estimated rates in the order of magnitude. It cannot always be concluded from such agreements between analytical and experimental results that the present analysis may be applied to the case of large Knudsen number for electrons, since the analysis is based on many assumptions and the data are not sufficient to draw any definite conclusions. However, one may expect that the energy transfer processes of an electron gas can be clarified to some extent by solving the energy equation for electrons as a continuum fluid even for the case when the Knudsen number for electrons is moderately large up to a certain value.

In the present paper, the exponential decay rate of the electron temperature along the tube axis is obtained in an analytical formula, and the analytical results are partly supported by the experimental works.

Acknowledgement

The author would like to express his sincere gratitude to Professor Hakuro Oguchi for his helpful guidance and encouragement during the progress of the present study.

Department of Aerodynamics and Structures
Institute of Space and Aeronautical Science
University of Tokyo, Tokyo
February 20, 1970

References

[1] Grewal, M. S. and Talbot, L.: J. Fluid Mech., **16** (1963) 573.
[2] Jaffrin, M. Y. and Probstein, R. F.: Phys. Fluids, **7** (1964) 1658.
[3] Jaffrin, M. Y.: Phys. Fluids, 8 (1965) 606.
[4] Hoffert, M. I. and Lien, H.: Phys. Fluids, **10** (1967) 1769.
[5] Nelson, H. F. and Goulard, R.: Phys. Fluids, **12** (1969) 1605.
[6] McNab, I. R. and Lindley, B. C.: Advances in MHD, McGraw-Hill, New York, (1963) 27.
[7] Bray, K. N. C.: The High Temperature Aspects of Hypersonic Flow, Ed. Nelson, W. C., Pergamon Press, New York, (1964) 67.
[8] Pai, S. I. and Tsao, C. K.: Z. Angew. Math. Phys., **16** (1965) 360.
[9] Talbot, Y. S., Chou, Y. S. and Robben, F.: Univ. California, Berkley, Rep. No. AS-65-14 (1965).
[10] Jukes, J.: Thesis, Graduate School of Aeronautical Engineering, Cornel Univ., (1956).

[11] Camac, M. and Kemp, N. H.: AIAA Preprint 63-460 (1963).
[12] Dix, D. M.: AIAA Journal, **2** (1964) 2081.
[13] Powers, J. O.: Ph. D. Thesis, Aerospace Engineering Dep., Univ. Maryland, College Park, Maryland (1965).
[14] Sherman, A. and Reshotko, E.: AIAA Journal, **7** (1969) 610.
[15] Gogosov, V. V.: PMM, **30** (1966) 512.
[16] Chung, P. M.: AIAA Journal, **3** (1965) 817.
[17] Schottky, W.: Z. Phys., **25** (1924) 635.
[18] Schottky, W. and Issendorff, J. V.: Z. Phys., **31** (1925) 163.
[19] Konenko, O. R.: (in Russian) Beschenik Moscovskovo unibersicheta, No. 5-1963 (1963).
[20] Goldstein, L. and Sekiguchi, T.: Phys. Rev., **109** (1958) 625.
[21] Sekiguchi, T. and Herndon, R. C.: Phys. Rev., **112** (1958) 1.
[22] Rotas, F., Bhattacharya, K. and Cahn, J. H.: Phys. Rev., **129** (1963) 495.
[23] Nygaard, K. J.: Phys. Rev., **157** (1967) 138.
[24] Pytte, A. and Winser, N. K.: ARL (Aerospace Research Lab., Air Force), 66-0047 (1965).
[25] Keefer, D. R.: AIAA Paper, 67-692 (1967).
[26] Randall, R. H. and Webb, H. W.: Phys. Rev., 48 (1935) 544.
[27] Baranov, V. Yu. and Vasil'eva, I. A.: High Temperature, **3** (1965) 155.
[28] Konenko, O. R.: High Temperature, **3** (1965) 145.
[29] Allis, W. P. and Rose, D. J.: Phys. Rev., **93** (1954) 84.
[30] Cohen, I. M. and Kruskal, M. D.: Phys. Fluids, 8 (1965) 920.
[31] Bohm, D.: The Characteristics of Electrical Discharge in Magnetic Fields, Eds. Guthrie, A. and Wakerling, R. K., McGraw-Hill, New York, (1949).
[32] Person, K. B.: Phys. Fluids, **5** (1962) 1625.
[33] Friedman, H. W.: Phys. Fluids, **10** (1967) 2053.
[34] Friedman, H. W. and Levi, E.: Phys. Fluids, **10** (1967) 1499.
[35] Shioda, S.: J. Phys. Soc. Japan, **27** (1969) 197.
[36] Biondi, M. A.: Phys. Rev., **93** (1954) 1136.
[37] Chung, P. M.: Phys. Fluids, **12** (1969) 1623.
[38] Burgers, J. M.: Plasma Dynamics, Ed. Clauser, F. H., Addison-Wesley, London, (1960) 119.
[39] Brown, S. C.: Basic Data of Plasma Physics 1966, MIT Press, Massachusetts, (1967) 13.
[40] Morse, T. F.: Phys. Fluids, **6** (1963) 1420.
[41] Daiber, J. W. and Waldron, H. F.: Phys. Rev., **151** (1966) 51.
[42] Fay, J. A.: AVCO Everette Research Lab. AMP 71 (1962).
[43] Shkarofsky, I. P.: Canad. J. Phys., **39** (1961) 1619.
[44] Johnson, E. O. and Malter, L.: Phys. Rev., **80** (1950) 58.
[45] Malter, L. and Webster, W. M.: RCA Rev., (1951) 191.
[46] Schlichting, H.: Boundary Layer Theory, Tr. Kestin, J., McGraw-Hill, New York, (1966) 231.
[47] Oskam, H. J. and Mittelstadt, V. R.: Phys. Rev., **132** (1963) 1445.
[48] Chen, C. L., Laiby, C. C. and Goldstein, L.: Phys. Rev., **121** (1961) 1391.
[49] Bates, D. R.: Phys. Rev., 78 (1950) 492.